GABRIEL ANGELO SARAIVA RAIMUNDO

FUNCTIONAL MODULATORS OF THE PRO-BEGOMOVIRAL PROTEIN NIG (NSP-INTERACTING GTPASE)

Dissertation submitted to the Genetics and Breeding Graduate Program of the Universidade Federal de Viçosa in partial fulfillment of the requirements for the degree of *Magister Scientiae*.

Adviser: Elizabeth Pacheco Batista Fontes

Co-advisers: João Paulo Batista Machado
Christiane Eliza Motta Duarte
Virgílio Adriano Pereira Loriato

VIÇOSA - MINAS GERAIS
2021

Ficha catalográfica elaborada pela Biblioteca Central da Universidade Federal de Viçosa - Campus Viçosa

T
R153f
2021

Raimundo, Gabriel Angelo Saraiva, 1996-
Functional modulators of the pro-begomoviral protein NIG (NSP-Interacting GTPase) / Gabriel Angelo Saraiva Raimundo. – Viçosa, MG, 2021.
1 dissertação eletrônica (71 f.): il. (algumas color.).

Texto em inglês.
Orientador: Elizabeth Pacheco Batista Fontes.
Dissertação (mestrado) - Universidade Federal de Viçosa, Departamento de Bioquímica e Biologia Molecular, 2021.
Referências bibliográficas: f. 51-61.
DOI: https://doi.org/10.47328/ufvbbt.2022.466
Modo de acesso: World Wide Web.

1. Begomovirus. 2. Proteínas. I. . II. Universidade Federal de Viçosa. Departamento de Bioquímica e Biologia Molecular. Programa de Pós-graduação em Genética e Melhoramento. III. Título.

CDD 22. ed. 579.28

Bibliotecário(a) responsável: Bruna Silva CRB-6/2552

GABRIEL ANGELO SARAIVA RAIMUNDO

FUNCTIONAL MODULATORS OF THE PRO-BEGOMOVIRAL PROTEIN NIG (NSP-INTERACTING GTPASE)

Dissertation submitted to the Genetics and Breeding Graduate Program of the Universidade Federal de Viçosa in partial fulfillment of the requirements for the degree of *Magister Scientiae*.

APPROVED: November 18, 2021

Assent:

Gabriel Angelo Saraiva Raimundo
Author

Elizabeth Pacheco Batista Fontes
Adviser

ACKNOWLEDGEMENTS

Primeiramente, agradeço aos meus pais Anderson e Marisa, e à minha irmã Maria Luiza pelos exemplos de comprometimento, esforço e amor, que sempre nortearam as minhas ações.

Agradeço às minhas avós Maria (*In memoriam*) e Luiza, e ao meu avô Alcides pelo carinho e suporte constantes.

Agradeço à família escolhida Filipe e Sálua pela paciência, amizade, conselhos e apoio diários, que me ajudaram a superar as dificuldades e incertezas agravadas pelo atual momento histórico.

Agradeço à minha orientadora Professora Elizabeth P. B. Fontes pelas contribuições para o meu desenvolvimento profissional. Agradeço por ter me recebido em seu laboratório ainda na graduação e pelas oportunidades de aprendizado ao longo do mestrado.

Agradeço ao meu coorientador Professor João Paulo B. Machado pelos ensinamentos e legado que me impulsionaram durante o desenvolvimento desta pesquisa.

Agradeço à minha coorientadora Professora Christiane E. M. Duarte, pela complacência com as minhas limitações e pelas diversas lições pessoais e científicas.

Agradeço ao meu coorientador Dr. Virgílio A. P. Loriato, pela contribuição técnica ao longo dos experimentos.

Agradeço ao Ruan Maloni Teixeira pela paciência, amizade, sinceridade e ovos de pato. Agradeço por desde sempre me ajudar a enxergar a sutileza dos fenômenos que se passam na bancada e fora dela.

Agradeço aos amigos do LBMP Gláucia, Iana, Lucas Ponte, Otto, Eduardo, Sâmera e Célio por toda ajuda, risadas e acolhimento durantes esses anos.

Agradeço ao professor Pedro Augusto B. dos Reis e aos colegas de LBMP Nívea, Nayara, Marco Aurélio, Nathália, Cleysinho, Igor, Dayane, Débora, Thainá, Laura, Eugênio, Phedra, Fredy, Márcia, Gustavo e Pedro Henrique pela convivência e momentos de aprendizado diários.

Agradeço aos excelentes amigos de Viçosa Juliana Abras, Gabriela Peterlini, Gabriela Soares, Fernanda Sardinha, Cauê, Lucas Daniel, Diego, Victor, Pollyanna, Paulo, João Paulo Herreira, Maria Alice, Luiza Campos e Roberta pela lealdade e companherismo.

Agradeço aos meus amigos Fernanda Rocha, Thábada, Guilherme, Bárbara, Larissa Portelote, Nayara e Luiza Vilas Boas, que mesmo distante também se fizeram presentes nos momentos chave.

Agradeço à Universidade Federal de Viçosa pela contribuição para a minha formação acadêmica.

Agradeço aos orgãos de fomento à pesquisa CNPq, CAPES e Fapemig, pelo apoio financeiro.

ABSTRACT

RAIMUNDO, Gabriel Angelo Saraiva, M.Sc., Universidade Federal de Viçosa, November, 2021. **Functional modulators of the pro-begomoviral protein NIG (NSP-Interacting GTPase).** Adviser: Elizabeth Pacheco Batista Fontes. Co-advisers: João Paulo Batista Machado, Christiane Eliza Motta Duarte and Virgílio Adriano Pereira Loriato.

The *Begomovirus* (*Geminiviridae* family) genome codes for multifunctional proteins responsible for viral replication, viral transport, subverting, and co-opting host functions to favor viral infections. The movement protein NSP (Nuclear Shuttle Protein) binds and escorts vDNA from the nucleus to the cytosol. The *Arabidopsis thaliana* cytosolic protein NIG (NSP-Interacting GTPase) accessorizes NSP transport from the nucleus to the cytosol. Accordingly, the overexpression of NIG confers enhanced susceptibility to begomovirus, thus placing NIG as a potential pro-begomoviral protein. Among host proteins, NIG associates with the endosomal NISP (NSP-interacting syntaxin domain-containing protein) to help NSP-vDNA traffic through the cytoplasm; and WWP1 (WW domain-containing protein 1), which entraps NIG in nuclear bodies. CSN5A (COP9 Signalosome Subunit 5a) is a potential NIG partner that has been shown to redirect it to the nucleus; however, NIG-CSN5A dynamic has not been elucidated. Since NIG partners influence its nuclear import, we examined whether some physiological stimulus could affect NIG localization. A phytohormone screening by confocal microscopy showed that salicylic acid (SA) could redirect NIG to the nucleus. Nuclear fractionation assays also indicated that SA could alter NIG localization to the nucleus. A *WWP1* Knockout line overexpressing NIG displayed the same confocal and nuclear fractionation pattern, indicating that SA-mediated transport was independent of WWP1-mediated nuclear import of NIG. Additionally, SA promoted NIG ubiquitination and degradation, a process prevented by the proteasome inhibitor MG132. To elucidate the underlying mechanism for the proteasome-mediated degradation of NIG, the interaction between NIG and CSN5A was further investigated. CSN5A negatively regulated NIG turnover and interacted with NIG *in vivo* by co-immunoprecipitation assays. In the absence of stimuli, the NIG-CSN5A complex was predominantly formed in the cytosol, as shown by the BiFC (Bimolecular Fluorescence Complementation) system, yet several lines of evidence were provided indicating that SA-mediated degradation of NIG may occur in the nucleus. First, SA mediated the nuclear

relocalization and degradation of NIG. Second, treatment with MG132 increased the SA-induced nuclear pool of NIG but did not alter the cytosolic levels of the protein. Finally, NIG formed a complex with CSN5A that participates in the proteolytic activity of the COP9 signalosome in the nucleus. To approach NIG role via reverse genetics, an *NIG* knockout line and independent complemented lines were obtained. Col-0, *NIG* knockout line, and NIG complemented lines were infected with the begomovirus CabLCV (Cabbage Leaf Curl Virus) through biolistics, but these genotypes did not display differences in resistance parameters against the begomovirus. These results complement the current knowledge on NIG functional modulators in the context of begomovirus infections, which may further elucidate the dynamic regarding this GTPase pro-begomoviral function.

Keywords: Begomovirus. NIG. NSP.

RESUMO

RAIMUNDO, Gabriel Angelo Saraiva, M.Sc., Universidade Federal de Viçosa, novembro de 2021. **Modeladores funcionais da proteína pró-begomoviral NIG (NSP-Interacting GTPase)**. Orientadora: Elizabeth Pacheco Batista Fontes. Coorientadores: João Paulo Batista Machado, Christiane Eliza Motta Duarte e Virgílio Adriano Pereira Loriato.

O genoma de *Begomovirus* (família *Geminiviridae*) codifica proteínas multifuncionais responsáveis pela replicação viral, transporte viral e cooptação das funções do hospedeiro para favorecer as infecções virais. A proteína de movimento NSP (*Nuclear Shuttle Protein*) se liga ao vDNA e auxilia o seu transporte do núcleo ao citosol. A proteína NIG, de *Arabidopsis thaliana*, é citoplasmática e assiste o movimento de NSP do núcleo para o citosol. Além disso, a superexpressão de NIG confere maior susceptibilidade a begomovírus, o que leva NIG a ser considerada uma proteína proviral. Dentre as proteínas do hospedeiro, NIG se associa com a proteína endossomal NISP (*NSP-interacting syntaxin domain-containing protein*) para acessorar o tréfego de NSP-vDNA pelo citoplasma; e WWP1 (*WW domain-containing protein 1*), que aprisiona NIG em corpos nucleares. CSN5A (*COP9 Signalosome Subunit 5A*) é um parceiro potencial de NIG capaz de redirecioná-la para o núcleo; no entanto, a dinâmica NIG-CSN5A não foi completamente elucidada. Visto que os parceiros de NIG influenciam a sua importação nuclear, avaliou-se se algum estímulo fisiológico poderia afetar a localização de NIG. Um *screening* de estímulos de fitohormônios monitorado por microscopia confocal com fitohormônios desmonstrou que o ácido salicílico (AS) poderia redirecionar NIG para o núcleo. Ensaios de fracionamento nuclear também indicaram que o AS poderia alterar a localização de NIG para o núcleo. Um nocaute de *WWP1* supexpressando NIG apresentou o mesmo de localização revelado pela microscopia confocal e fracionamento nuclear, indicando que o transporte mediado por AS é independente da importação de NIG mediado por WWP1. Adicionalmente, o AS promoveu a ubiquitinação e degradação da proteína NIG, um processo que foi impedido pelo inibidor do proteassomo MG132. Para elucidar o mecanismo de degradação de NIG mediada pelo proteassomo, a interação entre NIG e CSN5A foi investigada. CSN5A regulou negativamente a homeostase de NIG e também interagiu *in vivo* por ensaios de co-imunoprecipitação. Ensaios de BiFC (*Bimolecular Fluorescence Complementation*) demonstraram que na ausência de

estímulo, o complexo NIG-CSN5A foi predominantemente formado no citosol. No entanto, diversas evidências indicaram que a degradação de NIG mediada por AS pode ocorrer no núcleo. Inicialmente, a relocalização nuclear e a degradação de NIG foram influencidas pelo AS. Além disso, o tratamento com MG132 elevou o *pool* nuclear da proteína NIG induzido por AS, mas não alterou os níveis citosólicos da proteína. Finalmente, NIG formou complexo com CSN5A que participa da atividade proteolítica do signalosomo COP9 no núcleo. Para abordar o papel de NIG via genética reversa, um nocaute de *NIG* e linhagens independentes complementadas foram obtidos. Col-0, o nocaute de *NIG* e as linhagens comlementadas foram infectadas com o begomovírus CabCLV (*Cabbage Leaf Curl Virus*) via biolística, mas estes genótipos não apresentaram diferenças fenotípicas quanto aos parâmetros de resistência a begomovírus. Estes resultados complementam o atual conhecimento acerca dos moduladores funcionais de NIG contribuindo para desvendar a dinâmica que envolve NIG e sua função proviral.

Palavras-chave: Begomovirus. NIG. NSP.

LIST OF ILLUSTRATIONS

LIST OF TABLES

SUMMARY

1. INTRODUCTION

Geminiviruses are plant viruses that infect various crops and threaten food, feed, and fiber production, especially in tropical and subtropical environments. The *Geminiviridae* family consists of viruses that present a genome composed of circular single-stranded DNA, encapsidated by two geminated *quasi*-icosahedral virions, a structure represented by the Latin suffix "*Gemini*" that gave the name for this family of plant viruses (reviewed in Rojas *et al.* 2018). The geminiviral genome has six to eight genes, a small number compared to other phytopathogens such as bacteria, fungi, and nematodes. This limited proteomic variety is counterbalanced by multifunctional viral proteins that enable viral replication and the manipulation of both host and insect vector physiology, promoting efficient viral infection and propagation. The *Geminiviridae* family is composed of nine genera classified according to host, genome structure and organization, and phylogeny (reviewed in Rojas *et al.* 2018). The largest genus, *Begomovirus*, is transmitted to dicotyledonous plant species by the vector whitefly (*Bemisia tabaci*), a polyphagous Hemiptera (reviewed in Gilbertson *et al.* 2015).

The begomovirus genome may be either monopartite with one genomic component or bipartite with two components, and the related virus species occur mainly in the old and new world, respectively (reviewed in Rojas *et al.* 2005; Hanley-Bowdoin *et al.* 2013). In bipartite begomoviruses, the A component harbors five to six ORFs, which can be overlapped and code for proteins responsible for replication (Rep- and Ren), viral genes expression (TrAP), host RNAi immunity suppression (TrAP and AC4), and viral DNA (vDNA) encapsidation (CP-Coat Protein) (Zerbini *et al.* 2017). The B component has two ORFs coding for intra- and intercellular transport proteins: the NSP (Nuclear Shuttle Protein) and MP (Movement Protein). NSP interacts with vDNA and promotes its transit throughout the cytosol, whereas MP aids the translocation of the NSP-vDNA complex to neighbor cells through plasmodesmata (Gafni and Epel 2002; Lazarowitz and Beachy 1999; Noueiry, Lucas, and Gilbertson 1994; Sanderfoot and Lazarowitz 1995). The host-virus protein interaction studies are essential to understand better and manage plant resistance to viruses. The next chapter reviews the NSP interactions with host proteins, the relevance on the intracellular transport of vDNA, and the components of nucleocytoplasmic transport machinery subverted by intracellular viral movement.

2. REVIEW OF LITERATURE

2.1 NSP-host protein-protein interactions

Apart from its canonic transport function, the begomovirus component B virion-sense encodes BV1, also known as NSP, that interacts with host proteins within different compartments. While linked to vDNA, NSP recruits the acetylase nuclear shuttle interactor (NSI, At1g32070) to a ternary complex to acetylate the CP from *Cabbage Leaf Curl Virus* (CabLCV), which then dissociates from vDNA, favoring the vDNA-NSP interaction and the subsequent traffic of the complex to the cytosol (McGarry *et al.* 2003). This working model establishes a proviral role for the NSI enzyme, consistent with the higher infectivity by CabLCV in *NSI*-overexpressing *A. thaliana* lines (McGarry *et al.*, 2003). Carvalho and Lazarowitz (2004) showed that NSP-NSI interaction is mediated through 38-aminoacid peptide (residues 150 to 187) on the viral protein, in which the mutations E150G, I164T, and D187G are detrimental to NSP-NSI interaction but does not impair the canonic NSP properties, including nuclear localization, MP interaction, MP-influenced nuclear-cytosolic redirection, and ssDNA interaction. The NSP-E150G, I164T, or D187G CabLCV mutants displayed reduced infection rate, lower vDNA accumulation, and attenuated symptoms in Arabidopsis compared to wild-type CabLCV infection. These results further demonstrated the relevance of NSP-NSI interaction during begomoviral infection (Carvalho and Lazarowitz, 2004). NSP recruits and interacts with NSI within the same region required for self-interaction of the host protein. Therefore, NSP interaction debilitates NSI oligomerization and reduces its assembly into highly active NSI complexes, thereby partially compromising the natural NSI acetylation so that NSI is still capable of acetylating CP, but not as efficiently as its natural targets (Carvalho, Turgeon, and Lazarowitz 2006). NSI expression is predominant in young and/or sink tissues and vessels, raising the hypothesis that another layer of NSP interference over NSI function in plant development facilitates systemic viral infection (Carvalho, Turgeon, and Lazarowitz 2006).

Other targets for NSI acetylation are the core histones H3 and H2A, which interact via the basic residues with the vDNA phosphate backbone to form minichromosomes (Pilartz and Jeske 1992, 2003; McGarry *et al.* 2003). Zhou *et al.* (2011) proposed that H3 interacts simultaneously with vDNA and the movement proteins NSP and MP forming a movement-competent complex, in which the H3

packaging property assists the viral genome transport through the nucleoporin complex and subsequentially through plasmodesma. Therefore, the histone H3 acetylation by NSI might affect the NSP-H3 dynamic and constitute a critical posttranslational modification that influences these proteins in the course of begomovirus infection (McGarry *et al.* 2003; Zhou *et al.* 2011). The pleiotropic effects of manipulating the levels of core histones represent a challenging bottleneck to overcome in reverse genetics studies and for further comprehension of its interaction with NSP.

NSP also interacts with the NSP-Interacting leucine-rich-repeat receptor-like kinase (LRR-RLK), NIKs, from *Solanum lycopersicum*, *Glycine max*, and *A. thaliana* (Fontes *et al.* 2004; Mariano *et al.* 2004; Sakamoto *et al.* 2012). The *A. thaliana* homologs AtNIK1(At5g16000) and AtNIK3 (At1g60800) knockout (KO) lines showed significant susceptibility to begomoviruses. NSP from CabLCV and TGMV interacts with the activation loop of AtNIK1, AtNIK2 (At3g25560), and AtNIK3 and impairs their kinase activity. The conservation of NSP-NIK interactions between NSPs from different begomoviruses and NIK from diverse plant species suggests a mechanism in which NSP negatively modulates the host antiviral kinase receptors in an evolutive conserved way (Fontes *et al.* 2004). Among its targets, NIK1 mediates the phosphorylation of the cytosolic ribosomal protein L10 (RPL10a, At1g14320), leading to its translocation to the nucleus where it interacts with the transcription factor LIMYB (L10-Interacting MYB domain-containing protein), a critical repressor of translational machinery-related genes impairing host translation and thereby jeopardizing the viral protein synthesis (Carvalho *et al.* 2008c; Santos *et al.* 2009; Rocha *et al.* 2008; Zorzatto *et al.* 2015). Regarding NIK1 kinase activity, this RLK harbors positive T474 and inhibitory T469 phosphorylation-regulating residues. The phosphomimetic mutant T474D displays integral auto- and substrate phosphorylation activities whereas the loss-of-function mutation T469A leads to increased RPL10a phosphorylation (Santos *et al.*, 2009). The mutation T474D decreases NIK1-NSP binding affinity and precludes the substrate phosphorylation inhibition, promoting higher and constitutive RPL10a translocation to the nucleus, leading to the downregulation of ribosomal protein genes to the same level as in LIMYB-overexpressing lines. Collectively, these results demonstrate the mechanism by which NIK1 assemblies an antiviral defense response and the NSP inhibitory importance in begomoviral infection (Santos *et al.*, 2009; Zorzatto *et al.*, 2015). Teixeira *et al.* (2019) showed that vRNA and vDNA promote transcriptional

repression of the ribosomal proteins RPL13 and RPS25 similarly as observed in LIMYB-overexpressing and NIK1T474D-expressing plants, indicating these viral Pathogen Associated Molecular Patterns (PAMPs) as possible activators of the NIK1 pathway. Additional evidence demonstrated that the NIK1 closest homolog NIK2 acts redundantly and is activated by vRNA and vDNA to assemble an antiviral defense (Teixeira *et al*., 2019).

Tomato Yellow Spot Virus (ToYSV) NSP has also been shown to interact with the tomato BRI1 Associated Kinase1 (SlBAK1, Solyc10g047140) by yeast two-hybrid assay (Sakamoto *et al*., 2012) and with the NIK1 ortholog AtBAK1 or AtSERK3, which also interacts with other Leucine-Rich Repeat Receptor-Like Kinase (LRR-RLKs), Flagellin-Sensitive 2 (FLS2, At5g46330) (Chinchilla *et al*., 2011). FLS2 is activated by the flagellin bacterial PAMP and, in turn, phosphorylates BAK1, which activates PTI responses against bacteria and phosphorylates NIK1 at the position T474 leading to the activation of the NIK1 antiviral signal transduction (Li *et al.* 2019). The entire disclosure of the NSP-BAK1 connection may reveal another component of antiviral and antibacterial immunity cross-talk.

The PERK-like NSP-associated Kinase (NsAK) represents another kinase identified in an NSP-baited yeast two-hybrid screening, which has been demonstrated to phosphorylate NSP *in vitro.* NSP stably interacts with the NsAK inactive kinase domain (ΔKD) *in vitro* more efficiently than with the whole protein or the complete KD (Florentino *et al*., 2006). NsAK transcripts transiently accumulate and later decay after mechanical stress, *i.e*., rubbing and wounding, and after soil-borne fungus *Sclerotinia sclerotium* inoculation. Nevertheless, *NsAK* mRNA accumulation has not been detected in CabLCV or TCrLYV NSP-overexpressing plants and CabLCV-infected plants (Florentino *et al.* 2006). Additionally, the *NsAk* T-DNA insertional mutant line showed a lower infection rate when compared to the Col-0 ecotype, suggesting that NsAK somehow exhibits proviral function, possibly linked to the NSP posttranslational modification (Florentino *et al.* 2006).

Among genes linked to leaf anomalous development, the asymmetric leaves 2 (AS2, At1g65620) is upregulated by CabLCV infection via NSP (Ye *et al.* 2015). The viral protein NSP also interacts with and promotes AS2 traffic to the cytoplasm, where it is reallocated to the processing bodies (PBs) and passively modulates the catalysis of its partner Decapping 2 (DCP2, At5g13570). DCP2 is an mRNA decapping enzyme that binds to NSP, contributing to the hypothesis that NSP and AS2, and DCP2 act in

consonance to enhance the mRNA decapping activity (Xu *et al.* 2006; Thran *et al.*, 2012; Ye *et al.* 2015). The current model proposes that NSP enhances both the AS2 transcript levels and its cytosolic pool, contributing to its reallocation to PBs and DCP2 binding; thereby, activating DCP2 to lessen siRNA amount and hinder post-transcriptional gene silencing (PTGS), which finally favors the viral mRNA accumulation. This ongoing model is consistent with the higher and lower begomoviral virulence in AS2-overexpressing and *as2*-knockout lines, respectively (Ye *et al.*, 2015).

Li *et al.* (2014) reported that NSP from CabLCV directly interacts in the nucleus with the Jasmonate Insensitive 1 (JIN1 or MYC2, At1g32640), a transactivation factor that binds to the G-box cis-elements and upregulates the genes responsible for terpene synthesis such as Terpene Synthase 10 (TPS10, At2g24210) and Terpene Synthase 4 (TPS04, At1g61120). The *Tomato Yellow Leaf Curl China Virus* (TYLCCNV) βC1 protein has been shown to heterodimerize with the basic Helix Loop Helix (bHLH) domain of MYC2 and impair its dimerization and DNA binding, resulting in depleted levels of its downstream elements such as the terpene biosynthesis genes, *i.e.*, TPS10; and the jasmonic acid pathway genes, *i.e.*, VSP1; and the aliphatic and indole glucosinolates genes, i.e., *GSTF11* (Li *et al.*, 2014). Both monopartite TYLCCNV and bipartite CabLCV infections lead to lower terpene synthesis, resulting in better *Bemisia tabaci* performance (Li *et al.* 2014). As for MYC2, the insertional T-DNA knockouts in *A. thaliana* and VIGS-silenced lines in *N. benthamiana* exhibit lower levels of terpenes like α-bergamotene and β-myrcene, which mutualistically beneficiates the CabLCV vector *B. tabaci* attraction and oviposition. Terpenes function as an insecticidal, repellent, and natural enemy attractiveness, thus constituting an efficient strategy against *B. tabaci* (Luan *et al.* 2013; R. Li *et al.* 2014). Additional assays may contribute to better establishing BV1 as a βC1 analog in vector-plant interactions and the vector-virus synergism.

In mammals, the endoribonuclease Ras-GAP SH3 domain-binding protein (G3BP) homologs are listed among crucial proteins for stress granules (SGs) formation under stress conditions, including oxidative stress, heat shock, and viral infections (Tourrière *et al.* 2003; Panas *et al.* 2012). G3BP exhibits antiviral function due to the assembly of SGs, which negatively impacts host translation and viral protein translation during viral infections. This host defense mechanism is counteracted by different viral mechanisms to disrupt SGs, including the poliovirus proteinase 3C cleavage of G3BP (White *et al.* 2007) and the alphavirus SFV nsP3 interaction with G3BP through the

nsP3 carboxyterminal FGDF motif (Panas *et al.*, 2012, 2015). The key FGDF motif found in animal virus and host proteins propelled the search for identical or physicochemical similar motifs in plant virus-encoded proteins and their hosts (McInerney 2015; Panas *et al.* 2015; Krapp *et al.* 2017). In begomoviruses, the (F/Y)VS(F/Y) motif is conserved at the NSP carboxyterminal region. As hypothesized, NSPs from *Abutilon Mosaic Virus* (AbMV) and *Pea Necrotic Yellow Dwarf Virus* (PNYDV) interact *in vivo* and colocalize upon heat and salt stress with the G3BP-like (AT5G48650) (Krapp *et al.*, 2017). AbMV NSP presents a human G3BP homolog-related FVSF sequence, and the loss-of-function AASF mutant blocks the SG assembly (Krapp *et al.*, 2017). Although begomoviral NSP interacts with the G3BP-like protein, the relevance of this interaction remains elusive (Krapp *et al.* 2017).

2.2 The NSP Interacting GTPase and its potential roles

NIG (NSP-interacting GTPase, At4g13350), a cytosolic protein that facilitates the NSP-vDNA release from the nucleus to cytosol, is another relevant host protein that is modulated by begomoviruses (Carvalho *et al.*, 2008a,b). NIG has 602 amino acid residues and is a 65,6 kDa protein that interacts *in vivo* and *in vitr*o with different begomovirus NSPs, and exhibits biochemical and structural proprieties consistent with its potential role in the nucleus-cytoplasm transport of viral particles (Carvalho *et al.* 2008a). The NIG N-terminal domain is highly similar to hRIP (Rev-interacting protein), a human protein that interacts with the HIV Rev protein, constituting a cellular cofactor for the viral RNA movement from the nucleus periphery to the cytosol (Sánchez-Velar *et al.* 2004). Therefore, the HIV Rev role in humans is conceptually similar to the begomovirus NSP performance in plants. Both hRIP and NIG exhibit an N-terminal ArfGAP (ADP Ribosylation Factor – GTP Activating Protein) domain, common to vesicle, intracellular location, and signaling proteins (Chavrier and Goud 1999; Carvalho *et al.*, 2008; Spang *et al.*, 2010). Despite similarities between human hRIP and NIG, hRIP is localized in the nucleus of mammal cells, while Arabidopsis NIG is a cytosolic protein located around the nucleus. The *A. thaliana* genome has two proteins that share similarities with NIG, encoded by the loci At1g08680 and At4g32630, which share 43 and 40% sequence identity with full-length NIG, and 75 and 71,4% of identity, respectively, with the ArfGAP domain (Carvalho *et al.* 2008a).

Although NIG may participate in the nucleocytoplasmic transport of plant proteins, the only protein known to interact with NIG in the nucleus is the nuclear-

localized WW domain-containing protein 1 (WWP1, At2g41020). The tryptophan domains are essential for WWP1 interaction with NIG, binding to vDNA, and nuclear bodies formation (Calil *et al.* 2018). By sequestering NIG into the nuclear bodies, WWP1 prevents the NSP-NIG traffic to the cytosol, providing an antiviral function, consistent with enhanced resistance displayed by *WWP1*-overexpressing lines and the higher susceptibility to CabLCV infection exhibited by *atwwp1* knockout lines (Calil *et al.* 2018). Antagonistically, the vDNA can dismantle the WWP1-mediated nuclear bodies assembly, showing that viruses coopt the NIG protein and modulate its partner WWP1 (Calil *et al.*, 2018).

NIG also displays an essential dynamic interaction with NSP-interacting syntaxin domain-containing protein (NISP, At4g30204) (Gouveia-Mageste *et al.*, 2021). The endosomal protein NISP has been first identified from a microarray screening that mapped possible components of the NSP-protein interaction hub. Further investigation demonstrated that the NSP-NISP interaction happens through the NISP aminoterminal syntaxin-6 domain. NISP shares with its full-length paralog (At2g18860) 60,9% identity, and 78,57% identity within the syntaxin-6 domain of the proteins. Despite the high conservation of sequence, the NISP paralogs were inefficient in interacting with NSP. NISP also directly binds vDNA and NIG. Interaction between NIG and NISP is enhanced by the presence of NSP. Additionally, NISP colocalizes with the synaptogamin SYTA, an endosomal protein that regulates the MP transport via plasmodesmata (Lewis and Lazarowitz 2010). The structural and functional features of NISP along with its described interactions support a mechanistic model for intracellular transport of vDNA, in which NISP contributes to the traffic of vDNA by recruiting the NIG-NSP-vDNA complex to vesicles, where opportunistically MP, recruited by SYTA to the vesicles, forms the vDNA-NSP-MP complex, to be delivered to adjacent cells via plasmodesmata. Since NISP escorts the vDNA shuttle from the nucleus to the cell periphery and, thereby, promotes systemic infection, it is classified as a pro-begomoviral host protein. Accordingly, the *nisp-1* knockout line displays enhanced resistance against begomoviruses in contrast to the overexpressing lines that are more susceptible to infection (Gouveia-Mageste *et al.* 2021)

The NIG cellular function has not been completely elucidated, which may depend on the scrutiny of its interactome and its regulation upon virus infection. Besides WWP1 and NISP, the protein CSN5A (COP9 Signalossome Subunit 5A, At1g22920) has also been demonstrated to interact with NIG (Machado 2011). This

signalosome component displays catalytic activity that positively controls the deneddylation of the culin-RING subunit of E3 ligases favoring the substrate polyubiquitination(Cope *et al.* 2002; Rabut and Peter 2008; Merlet *et al.* 2009). Other putative NIG interactions are the E3 ligases At5g04460 and At3g05545 (Machado, 2011), which may be associated with a proteasome-mediated degradation pathway targeting NIG. Additionally, confocal microscopy assays indicated that CSN5A could influence the NIG traffic to the nucleus; however, the CSN5A/NIG dynamic has not been fully characterized (Machado 2011). CSN5A can occur both in the cytosol as a monomer and in the nucleus associated with other signalosome subunits; thereby, CSN5A mediates its targets degradation within the nucleus (Kwok *et al.* 1998; reviewed in Wei, Serino and Deng 2008; reviewed in Jin *et al.* 2014). Since NIG is a cytosolic GTPase, it remains elusive where the CSN5A-NIG interaction takes place. Furthermore, the biological significance of the complex formation for NIG antiviral and cellular functions has yet to be elucidated.

2.3 Nucleocytosolic transport of proteins

Distinct shuttle mechanisms accompany the eukaryote cell compartmentalization amid the subcellular divisions, and fine-tuning these active transport mechanisms are essential to steady-state maintenance and stress responses. The nucleocytoplasmic transport occurs through the nuclear pore complex (NPC), a structure that permeates the nuclear envelope and is characterized by an eight-fold radial symmetry composed of over 30 different nucleoporins (Nups) (reviewed in Dirk and Kutay, 1999; Li and Gu, 2020). The NPC native conformation, when depleted of membrane and interacting partners, has about 52 MDa. Nups are classified as (i) the transmembrane Nups, which adhere the NPC to the nuclear envelope, (ii) scaffold Nups, which compose the NPC structural core rings to which nuclear baskets and cytoplasmic structures are attached, and (iii) FG Nups, fixed on the core scaffold, facing the NPC channel and responsible for transport selectively (Alber *et al.* 2007; Zhou, Boruc, and Meier 2013; Kim *et al.* 2018).

The NPC channel allows passive diffusion of ions, small metabolites, water, and proteins with a molecular weight below the 40kDa range, even if slowly. In contrast, larger proteins depend on the active transport mediated by the nuclear transport receptors (NTRs) importins and exportins, which in consonance with RanGTPase mediate the bidirectional transport between nucleoplasm and cytoplasm (reviewed in

Tamura and Hara-Nishimura 2014; Zhou, Boruc, and Meier 2013). According to the RanGTP system, importins interact with the cargo proteins in the cytosol through its nuclear localization signal (NLS) and promote their traffic to the nucleus. Inside the nucleus, the importins bind to RanGTP, change their conformation and release the cargoes to return to the cytoplasm as RanGTP-bound importins. GTP is hydrolyzed to GDP in the cytosol, leading to the dissociation of RanGDP and importins, thus allowing another cycle to begin. Conversely, the RanGDP-bound exportin shuttles to the nucleus, where GDP is exchanged by GTP, and then RanGTP-bound exportin cooperatively interacts with the cargo through its nuclear export signal (NES). The cargo-exportin-RanGTP complex is then transported to the cytosol, where RanGTP is converted to RanGDP, thus dismantling the complex affinity, to recycle the exportin and release the cargo (Zhou *et al.*, 2013 reviewed in Cavazza and Vernos, 2016). The directionality of this process is guaranteed by the presence of Ran GTPase Activating Protein (RanGAP) in the cytosol and Ran Guanine nucleotide Exchange Factor (RanGEF) in the nucleus, promoting higher RanGDP concentrations in the cytosol and higher accumulation of RanGTP in the nucleus (Cavazza and Vernos, 2016).

Both importin and exportin-meditated processes within the RanGTP pathway lead to the export of RanGTP from the nucleus, which could conceptually be counterbalanced by Ran diffusion to the nucleoplasm since it has 24 kDa, and hence fits the requirement for passive diffusion through the NPC (Dirk and Kutay, 1999). However, this diffusion occurs at a low rate and is catalyzed by NTF2 (Nuclear transport factor 2), which binds to RanGDP in the cytosol and promotes its translocation to the nucleus, where it is converted to RanGTP by a RanGEF enzyme (Smith, Brownawell, and Macara 1998; Ribbeck *et al.* 1998).

Despite the specificity and directionality assured by the Nups and the associated proteins, additional regulation steps are needed to calibrate the traffic between nucleoplasm and cytoplasm (reviewed in Christie *et al.*, 2016). Among different regulation mechanisms, phosphorylation represents a significant posttranslational modification (PTMs), which affects the nucleocytoplasmic trafficking of shuttle proteins. Besides other less common PTMs, including acetylation, methylation, ubiquitination, and SUMOylation, phosphorylation may augment or reduce the cargo binding affinity to the importin via inter or intramolecular masking of the NLS and through organelle-specific retention (Christie *et al.*, 2016). Additionally, the nuclear import of cargoes can be positively affected by the number of NLSs within

their structure; or be affected via microtubular transport to perinuclear regions with higher concentrations of importins, thereby, with increased shuttle rate to the nucleus. Nuclear importation can also be affected by piggy-back processes, characterized by the co-transport of proteins deprived of NLS, which, however, interact with another protein containing one or more NLSs (Christie *et al.*, 2016).

Although NIG can be sequestered by WWP1 in nuclear bodies and be redirected to the nucleus by CSN5A, the underlying mechanism for NIG relocation and whether other stimuli may influence NIG shuttling are still unknown (Calil *et al.* 2018; Machado 2011).

Given the relevance of regulated nucleocytoplasmic traffic in eukaryotic cells, the present work evaluated whether any plant hormones could activate the NIG nucleocytoplasmic transport and its effect on begomovirus infection. Biochemical assays were carried out to further confirm NIG and CSN5A interaction *in vivo*. Additionally, NIG knockout lines and complemented lines were obtained, and their resistance against begomovirus was evaluated by reverse genetics.

3. MATERIALS AND METHODS

3.1 Plasmid Constructs

The recombinant plasmids deployed in this work were previously produced via Gateway® cloning system (Thermo Fisher Scientific™) by the Laboratório de Biologia Molecular de Plantas (LBMP) research group.

The NIG clones in entry vectors were made by Carvalho *et al.* (2008a) and assigned as NIG-NS-pDONR201 and NAP-St-pDONR207(pUFV1083). Machado (2011) obtained NIG-NS-pDONR207 (pUFV1643) the CSN5A into the entry vectors, resulting in CSN5A-NS-pDONR201(pUFV1436) and CSN5A-NS-pDONR207 (pUFV 1645). The respective ORFs were transferred from the entry vectors to plant expression plasmids. Carvalho *et al.* (2008a) produced the clones pK7F-NIG and YFP-NIG (pUFV1085), harboring 35S::NIG-GFP and 35S::YFP-NIG fused ORFs into the vectors pK7FWG2 and 35S-YFP-casseteA-Nos- pCAMBIA1300. Machado (2011) inserted CSN5A into the expression vector pK7FWG2 producing CSN5A-NS-pK7FWG2 (pUFV1447), which harbors 35S::CSN5A-GFP.

In all constructs, the transient or stable expression in plants of the recombinant gene was controlled by the CaMV promoter 35S. For co-immunoprecipitation (Co-IP) assays, the ORFs of NIG and CSN5A were fused to GFP (Green Fluorescent Protein) and HA (Hemagglutinin) tags, under the control of the 35S promoter. The combinations used were 2x35S::NIG-6HA (pUFV2221), 35S::NIG-GFP, 2x 35S::CSN5A-6HA (pUFV2223), 35S::NIG-GFP and eGFP (pUFV1088). The constructs 2x35S::NIG-6HA, 2x 35S::CSN5A-6HA and eGFP were also previously produced by the LBMP research team.

The vectors used in Bimolecular Fluorescence Complementation (BiFC) assays were obtained by transferring the inserts of NIG-pDONR207 and CSN5A-pDONR207 to the expression vectors SPYCE-GW and SPYNE-GW; thereby obtaining NIG-SPYCE (pUFV1647), NIG-SPYNE (pUFV1646), CSN5A-SPYCE (pUFV1649) and CSN5A-SPYNE (pUFV 1648). Each of these two expression vectors contains a fragment of Yellow Fluorescent Protein (YFP): SPYCE harbors the C-terminal (cYFP, pUFV1642) and SPYNE has the N-terminal (nYFP, pUFV1641) region.

3.2 Plant Material and Growth Conditions

All assays with plants were performed with the model plant species *Arabidopsis thaliana* and *Nicotiana benthamiana.* The *A. thaliana* Columbia (Col-0) was utilized as wild type, whereas the T-DNA insertional mutants SALK_014974 (*atnig-1*) and SALK_073780C (*atwwp1-1*; Calil *et al.,* 2018) were genotyped as *nig* and *wwp1* knockout lines, respectively.

The Col0/35S::NIG-GFP line was previously obtained and described by Carvalho (2008a). The Col0/35S::NIG-GFP was previously obtained and characterized by the LBMP research group. The *atwwp1*/35S::YFP-NIG, *atnig*/35S::YFP-NIG, Col0/2x35S::NIG-HA, and Col0/35S::CSN5A-GFP lines were obtained by the floral dipping method (Zhang, 2006). To produce *atwwp1*/35S::YFP-NIG and *atnig*/35S::YFP-NIG, both *atwwp1-1* and *atnig-1* flowers were submersed into *Agrobacterium tumefaciens* GV3101 transformed with the construct 35S::YFP-NIG, while Col-0 was transformed with 2x35S::NIG-HA and 35S::CSN5A-GFP via Agrobacterium-mediated transformation, thus yielding Col0/2x35S::NIG-HA and Col0/35S::CSN5A-GFP.

The seeds from T0 and following generations were selected in Murashige and Skoog (MS)-containing phytagel plates supplemented with sucrose and Hygromycin (10mg/L) or Kanamycin (100mg/L). The plates were placed in the dark at 4ºC for 72 hours and then put in the growth chamber for 14 days at 22 ºC and photoperiod of 16h light/ 8 h dark. The selected plants were transferred to the soil. The transgenic lines harboring 35S::YFP-NIG or 2x35S::NIG-HA were confirmed by PCR with the primers MC36 and the ArfGAP-rvs (Table S1), while the lines containing the construct 35S::CSN5A-GFP were confirmed using the primers MC36 and CSN5A-NS-Rvs (Table S1).

The seeds of *Nicotiana benthamiana* plants were germinated in soil and grown under 25 ºC and photoperiod of 16h light/ 8h dark in the greenhouse.

3.3 Confocal microscopy imaging of *N. benthamiana* leaves treated with leptomycin B

The vector NIG-GFP was used to transform *A. tumefaciens* strain GV3101. Transformed GV 3103 colonies were inoculated into LB liquid medium at 28ºC for 16 h, pelleted at 2500 x *g* for 5 min, and washed with the infiltration buffer 3 times [10 mM MgCl2, 10 mM MES pH 5,6, 400 µM acetosyringone] and resuspended to an OD_{600nm}

= 1. The *A. tumefaciens* transformed with NIG-GFP was infiltrated into *N. benthamiana* abaxial leaves. The treatment 100nM Leptomycin B diluted in 100mM MES and 10mM $MgCl_2$ was applied 3 h before analysis.

The epidermal cells of agroinfiltrated areas were analyzed after 72 hours with a Zeiss inverted LSM510 META laser scanning microscope equipped with argon and helium lasers as excitation sources. The NIG-GFP fusion protein was excited at 488 nm with the argon laser, and GFP emission was detected using a 500-530 nm filter. The images were captured and processed with the Zeiss LSM Image Browser 4 software.

3.4 Confocal microscopy imaging of *Arabidopsis thaliana* roots

Seedlings of Col0/35S::NIG-GFP and *atwwp1*/35S::YFP-NIG were surface sterilized and placed in phytagel plates supplemented with MS and sucrose for 3 to 4 days. Col0/35S::NIG-GFP were incubated in 100 µM and 500 µM Salicylic Acid (SA), 100 µM Methyl Jasmonate (MeJA), 100 µM 1-Aminocyclopropane 1-Carboxylic Acid (ACC), 10 µM 2,4-Dichlorophenoxyacetic Acid (2,4-D) and 100µM Abscisic Acid (ABA) solutions for 20 to 24 h. The *atwwp1*/35S::YFP-NIG seedlings were incubated in SA 500 µM 6h before the confocal microscopy analysis with a Zeiss inverted LSM510 META laser scanning microscope equipped with an argon laser and a helium laser as excitation sources. The GFP protein was excited at the 488 nm interval and the fluorescence was detected at 500–530nm. The YFP-fused protein was excited at 514 nm with the argon laser, and YFP emission was detected using a 560-615 nm filter. The images were captured and processed with the Zeiss LSM Image Browser 4 software.

3.5 SA effect on NIG subcellular localization

The *A. thaliana* transformants Col0/35S::NIG-GFP and Col0/2x35S::NIG-HA were used in this assay. The seeds were surface sterilized, and placed in phytagel plates supplemented with MS and sucrose. The plates were placed in the dark at 4ºC for 72 hours, and then incubated in the growth chamber for 14 days at 22 ºC and photoperiod of 10h light/ 14h dark. The seedlings were carefully placed in 12 wells plates filled with liquid $MS^1/_4$ strength medium (1 mL/ well). Around 10 seedlings were put in each well and the plates were placed for 48h in the growth chamber with 10 h light/ 14 h dark photoperiod. The MS medium was removed and 1 mL of 500 µM

cycloheximide was added. After 2 h, MG132 diluted in DMSO was added to a final concentration of 30 µM. Control samples were treated with the same volume (3 µL) of the solvent DMSO without MG132. After 1 h, SA was added to a final concentration of 500 µM. Control samples not treated with SA had an equivalent DMSO volume added (5µL).

The genotype Col0/2x35S::NIG-HA samples were collected at 0, 3, 6, 9 and 12 hours after incubation with SA, while the samples of the genotype Col0/35S::NIG-GFP were collected at 0, 3, 6 and 9 hours post treatment. Samples of 200 mg were put in microtubes and ground with sterilized metal spheres in a Tissue Lyser II (Qiagen). Total protein was extracted with 200 µL of buffer [50 mM Tris-HCl pH 8,0, 1 % (v/v) NP-40, 2 mM PMSF, 2 mM Benzamidine] and the samples were gently agitated for 30 min and centrifuged at 10000 x *g* for 10 min. Total protein was quantified through the Bradford method and aliquots of 100 ng were resolved on 10% (w/v) SDS-PAGE gel, transferred to nitrocellulose membrane and immunoblotted with Rabbit anti-HA (Invitrogen, 71-5500) and Rabbit anti-GFP (Invitrogen, A11122). As an internal control, Rabbit anti-Actin and Rabbit anti-UGPase (Agrisera, AS05 086) antibodies were deployed. The membranes were washed 3 times with TBS-T for 10 minutes and incubated with Goat Anti-Rabbit-HRP (Invitrogen, 65-6120) conjugated antibody. The detection was performed with the SuperSignal™ West Dura Extended Duration Substrate, according to the manufacturer's instructions via the ChemiDoc® photodocumentator (Bio-Rad™). The bands corresponding to NIG-HA protein and the endogenous control UGPase were quantified via ImageJ software. For each quantification, the higher values of NIG-HA/UGPase ratio were equaled to 1 and the other values were normalized.

3.6 Determination of Posttranslational modifications

The *A. thaliana* transformant Col0/2x35S::NIG-HA was utilized in this assay. The seeds were surface sterilized, sawed in phytagel plates supplemented with MS and sucrose. The plates were placed in the dark at 4°C for 72 hours, and then transferred to a growth chamber for 14 days at 22 °C and 10h light/ 14 h dark photoperiod. The seedlings were carefully placed in 12 wells plates filled with MS 1/4 strength medium 1mL / well. Around 10 seedlings were put in each well and the plates were placed for 48h in the growth chamber with 10h light/ 14 h dark light conditions. The MS medium was removed and 1 mL of sterile water was added. MG132, diluted

in DMSO was added to a final concentration of 30 µM. After 1h, SA was added to a final concentration of 500 µM and incubated for 8h. The samples that were not treated with SA had an equivalent DMSO volume added (5 µL). Samples (400 mg) were collected and ground with liquid nitrogen and then mixed with 1 mL of protein extraction buffer [50 mM Tris-HCl pH 8,0, 1% (v/v) NP-40, 2 mM PMSF 2 mM Benzamidine] supplemented with 100 µM MG132 and phosphatase and protease inhibitors 25mM NaF and cOmplete® . The samples were gently agitated for 30 min and centrifuged at 10000 x *g* for 10 min. The protein extracts were incubated for 2 h with 50 µL anti-HA beads (MACS/ Miltenyi Biotec) at 4ºC under gentle rotation. The extracts were applied to a MACS column and washed and eluted with 50 µL of elution buffer pre- heated at 95ºC. Before the incubation with beads, the samples were quantified via the Bradford method and aliquots of 100 ng were prepared from all samples to use as input control. The Immunoprecipitate (IP) eluates and inputs were resolved in 10% (w/v) SDS-PAGE gel and then transferred to nitrocellulose membrane. The input was immunoblotted with Rabbit anti-HA (Invitrogen, 71-5500) and anti-UGPase (Agrisera, AS05 086). The IP membrane was probed with Rabbit anti-HA (Invitrogen, 71-5500), Mouse Anti-Ubq (Santa Cruz Biotechnology, (P4D1) sc-8017), Rabbit anti-phosphoserine-HRP (Sigma, SAB5200087), Rabbit anti-phosphotyrosine-HRP (Sigma, 61-5800) and Rabbit anti-phosphothreonine antibodies. A single blot was analyzed sequentially with different antibodies by washing the membrane with the stripping solution [200 mM glycine, 0,1 % (w/v) SDS, 1% (v/v) tween] followed by one PBS 1X wash and two TBS-T washes. The detection was performed with the SuperSignal™ West Dura Extended Duration Substrate, according to the manufacturer's instructions via the ChemiDoc® photodocumentator (Bio-Rad™).

3.7 Nuclear fractionation

This protocol for nuclear fractionation was adapted from Yamauchi *et al.* (2014). The *A. thaliana* transformants Col0/35S::NIG-GFP, Col0/2x35S::NIG-HA and *atwwp1-1*/YFP-NIG were used in this assay. The seeds were surface sterilized, sawed in phytagel plates supplemented with MS and sucrose. The plates were placed in the dark at 4ºC for 72 hours, and then transferred to the growth chamber for 14 days at 22 ºC and photoperiod of 10h light/ 14 h dark. The seedlings were carefully placed in 12 wells plates filled with MS 1/4 strength medium 1 mL / well. Around 10 seedlings were put in each well and the plates were placed for 48 h in the growth chamber with 10 h

light/ 14 h dark light conditions. The MS medium was removed and 1 mL of sterile water was added. MG132 was added to a final concentration of 30 µM. Control samples were treated with the same volume (3 µL) of the solvent DMSO without MG132. After 1 h, SA was added to a final concentration of 500 µM. The samples that were not treated with SA had an equivalent DMSO volume added (5 µL).

The samples were weighted to 400 mg, ground in liquid nitrogen and ground in 600 µL of Nuclear Extraction Buffer [100 mM MOPS pH 7,6, 10 mM MgCl2, 0,25 M sucrose, 5% dextran T-40, 2,5% Ficoll 400,40 mM 2-Mercaptoetanol] supplemented with protease inhibitor cOmplete® and 100 µM MG132. The extract was filtered in 100 µm nylon and centrifuged at 12000 x *g* for 5 min. The supernatant, which corresponds to the cytosol fraction, was removed and quantified via the Bradford method. The microtubes were centrifuged again at 12000 x *g* for 5 min to remove the excess of supernatant adhered to the microtubes walls. Due to the low concentration obtained, the cytoplasmic fraction was concentrated to half volume with a SpeedVac™ Concentrator (Savant).

The pellet, that correspond to the nuclear fraction, was resuspended in 60 µL of Nuclei Lysis Buffer [50 mM Tris-HCl pH 8,0, 10 mM EDTA pH 8,0, 1% SDS] supplemented with protease inhibitor cOmplete® and 100 µM MG132. Samples were kept in ice for 30 min and agitated at every 10 min interval. The samples were then resuspended in 120 µL of protein extraction buffer [50 mM Tris-HCl pH 8,0 1% (v/v) NP-40, 2mM PMSF, 2 mM Benzamidine] supplemented with protease inhibitor cOmplete® and 100 µM MG132. The nuclear and cytosol fractions were resolved on 10% (w/v) SDS-PAGE gel, transferred to nitrocellulose membrane and immunoblotted with Rabbit anti-HA (Invitrogen, 71-5500) and Rabbit anti-GFP (Invitrogen, A11122). The samples were previously quantified and at least 50ng of each were applied. As for loading and contamination control between fractions, Rabbit anti-UGPase (Agrisera, AS05 086) and mouse Anti-RNApolII (Sigma, 087K0498) antibodies were deployed. The membranes were washed 3 times with TBS-T for 10 min and incubated with Goat Anti-Rabbit-HRP (Invitrogen, 65-6120) and goat anti-mouse-HRP (Santa Cruz Biotechnology, sc-2005) conjugated antibodies. The detection was performed with the SuperSignal™ West Dura Extended Duration Substrate, according to the manufacturer's instructions via the ChemiDoc® photodocumentator (Bio-Rad™).

3.8 CSN5A-mediated turnover of NIG

The vectors NIG-HA, CSN5A-GFP and eGFP were used to transform *A. tumefaciens* strain GV3101. Transformed GV 3103 colonies were inoculated into LB liquid medium at 28ºC for 16 h, pelleted at 2500 x *g* for 5 min and washed with the infiltration buffer 3 times [10 mM MgCl2, 10 mM MES pH 5,6, 400 µM acetosyringone] and resuspended to an OD_{600nm} = 1. Different combinations of the Agrobacterium suspensions were co-infiltrated into *N. benthamiana* abaxial leaves at a ratio 1:1. The combinations were: 1) CSN5A-GFP + NIG-HA; 2) NIG-HA, 3) eGFP + NIG-HA; 4) CSN5A-GFP + NIG-HA + 50 µM MG132 12 h prior to sample collection; 5) CSN5A-GFP + NIG-HA + 100 µM MG132 72h before collection, 6) CSN5A-GFP + NIG-HA + 100 µM MG132 18h before collection. The MG132 was diluted in 10 mM $MgCl_2$ solution.

After 72 hours of agroinfiltration, infiltrated leaf pieces (200 mg) were collected, ground in liquid nitrogen and ground with 1 mL of protein extraction buffer [50 mM Tris-HCl pH 8,0, 1% (v/v) NP-40, 2 mM PMSF, 2 mM Benzamidine, 100µM MG132]. The samples were gently agitated for 30 min and centrifuged at 10000 x *g* for 10 min. Aliquots of 30 µL were resolved on 10% (w/v) SDS-PAGE gel, transferred to nitrocellulose membrane and immunoblotted with Rabbit anti-HA (Invitrogen, 71-5500) and Rabbit anti-GFP (Invitrogen, A11122). The membranes were washed 3 times with TBS-T for 10 min and incubated with Goat Anti-Rabbit-HRP (Invitrogen, 65-6120) conjugated antibody. The detection was performed with the SuperSignal™ West Dura Extended Duration Substrate, according to the manufacturer's instructions via the ChemiDoc® photodocumentator (Bio-Rad™).

3.9 Bimolecular Fluorescence Complementation (BiFC) assay

The vectors NIG-SPYNE, NIG-SPYCE, CSN5A-SPYNE, CSN5A-SPYCE and empty SPYNE and SPYCE were used to transform *A. tumefaciens* strain GV3101. Transformed Agrobacterium colonies were inoculated into LB liquid medium at 28ºC for 16 h, pelleted at 2500 x *g* for 5 min, washed with the infiltration buffer 3 times [10 mM $MgCl_2$, 10 mM MES pH 5,6, 400 µM acetosyringone] and resuspended to an OD_{600nm} = 1. Different combinations of the Agrobacterium inoculum were co-infiltrated into *N. benthamiana* abaxial leaves at a ratio 1:1. The combinations were: pSPYNE-CSN5A + pSPYCE-NIG; pSPYCE-CSN5A + pSPYNE-NIG; pSPYCE-CSN5A +

pSPYNE, pSPYNE-CSN5A + pSPYCE, pSPYCE-NIG + pSPYNE, pSPYNE-NIG + pSPYCE.

The epidermal cells of agroinfiltrated areas were analyzed after 48 hours with a Zeiss inverted LSM510 META laser scanning microscope equipped with argon and helium lasers as excitation sources. The YFP-fused protein was excited at 514 nm with the argon laser, and YFP emission was detected using a 560-615 nm filter. The images were captured and processed with the Zeiss LSM Image Browser 4 software. As an additional control, some samples were previously treated with the proteasome inhibitor 100 µM MG132 18 h prior to the analysis. The MG132 was diluted in 10mM $MgCl_2$ solution.

3.10 Co-Immunoprecipitation (Co-IP) assay

The vectors containing NIG-GFP, NIG-HA, CSN5A-GFP, CSN5A-HA and eGFP were used to transform *A. tumefaciens* strain GV3101. Transformed colonies were inoculated into LB liquid medium at 28ºC for 16 h, pelleted at 2500 x *g* for 5 min, washed with the infiltration buffer 3 times [10 mM MgCl2, 10 mM MES pH 5,6, 400 µM acetosyringone] and resuspended to an OD_{600nm} = 1. Different combinations of the resuspensions were co-infiltrated into *N. benthamiana* abaxial leaves at a ratio 1:1. The combinations were: 1) CSN5A-GFP + NIG-HA; 2) NIG-HA; 3) eGFP + NIG-HA; and 4) NIG-GFP + CSN5A-HA; 5) CSN5A-HA; 6) eGFP + NIG-HA.

The leaf samples were previously treated with the proteasome 100µM inhibitor MG132 18 h before analyzing. The MG132 was diluted in 10mM $MgCl_2$ solution. After 72 h, 200 mg of infiltrated leaves were ground in liquid nitrogen and ground with 1 mL of protein extraction buffer [50 mM Tris-HCl pH 8,0, 1% (v/v) NP-40, 2 mM PMSF, 2 mM Benzamidine, 100 µM MG132]. The extracts were agitated for 30 min and centrifuged at 10000 x *g* for 10 min. The protein extracts were incubated for 2 h with 50 µL anti-GFP beads (MACS/ Miltenyi Biotec) at 4ºC under gentle rotation. The extracts were applied to a MACS column and washed and eluted with 50 µL of elution buffer pre-heated at 95ºC. Before the incubation with beads, two 30 µL aliquots were isolated from all samples to use as input control.

The input and IP samples were resolved on 10% (w/v) SDS-PAGE gel, transferred to nitrocellulose membrane and immunoblotted with Rabbit anti-HA (Invitrogen, 71-5500) and Rabbit anti-GFP (Invitrogen, A11122). The membranes were washed 3 times with TBS-T for 10 min and incubated with Goat Anti-Rabbit-HRP

(Invitrogen, 65-6120) conjugated antibody. Immunoblotted proteins were detected with the SuperSignal™ West Dura Extended Duration Substrate, according to the manufacturer's instructions via the ChemiDoc® photodocumentator (Bio-Rad™).

3.11 NIG-HA and endogenous CSN5A Co-IP

The *A. thaliana* transformant Col0/2x35S::NIG-HA was utilized in this assay. The seeds were surface sterilized, sawed in phytagel plates supplemented with MS and sucrose. The plates were placed in the dark at 4ºC for 72 h, and then transfer to the growth chamber for 14 days at 22 ºC and photoperiod of 10 h light/ 14 h dark. The seedlings were carefully placed in 12 wells plates filled with MS 1/4 strength medium 1 mL / well. Around 10 seedlings per well were placed for 48 h in the growth chamber with 10 h light/ 14 h dark light conditions. The MS medium was removed and 1mL of sterile water was added. MG132 diluted in DMSO was added to a final concentration of 30 µM. After 1 h, SA was added to a final concentration of 500 µM and incubated for 8 h. An equivalent DMSO volume added (5 µL) was added to the samples without SA.

Samples of 400 mg were collected and ground with liquid nitrogen and then mixed with 1 mL of protein extraction buffer [50 mM Tris-HCl pH 8,0, 1% (v/v) NP-40, 2 mM PMSF, 2 mM benzamidine, 100 µM MG132]. The samples were gently agitated for 30 min and centrifuged at 10000 *x g* for 10 min. The protein extracts were incubated for 2 h with 50 µL anti-HA beads (MACS/ Miltenyi Biotec) at 4ºC under gentle rotation. The extracts were applied to a MACS column, washed and eluted according to manufacturer's instructions. The elution was done with 50 µL of elution buffer pre-heated at 95ºC. Before the incubation with beads, the samples were quantified via the Bradford method and aliquots of 100 ng were prepared from all samples to use as input control. The Immunoprecipitate (IP) eluates and inputs were resolved in 10% (w/v) SDS-PAGE gel and then transferred to nitrocellulose membrane. The input was immunoblotted with Rabbit anti-HA (Invitrogen, 71-5500), Rabbit anti-CSN5A (Biomol Affiniti, Z04292) and anti-UGPase (Agrisera, AS05 086) antibodies. The IP membrane was probed with Rabbit anti-HA (Invitrogen, 71-5500) and Rabbit anti-CSN5A (Biomol Affiniti, Z04292). A single blot was sequentially reprobed by washing the membranes with stripping solution [200mM glycine, 0.1 % (w/v) SDS, 1% (v/v) tween] followed by PBS 1X wash and two TBS-T washes. The detection of immunoblotted proteins was performed with the SuperSignal™ West Dura Extended Duration Substrate, according

to the manufacturer's instructions via the ChemiDoc® photodocumentator (Bio-Rad™).

3.12 CabCLV infection assay

Plants from the of *A. thaliana* genotypes Col-0, *atnig-1* and the three complemented *atnig*/NIG were deployed in this assay. This experiment was also conducted with Col0 and two Col0/35S::NIG-GFP independent lines.

The seeds were surface sterilized, sawed in phytagel plates supplemented with MS and sucrose. The plates were placed in the dark at 4ºC for 72 h, and then put in the growth chamber for 14 days at 22 ºC and photoperiod of 10 h light/ 14 h dark. The seedlings were transferred to individual vases and after 14 days the plants were bombarded with the components A and B of the bipartite begomovirus CabLCV (*Cabbage Leaf Curl Virus*).

The infectious clones CabLCVA 007 and CabLCVB 002, containing tandem repeats of the viral genome, were extracted through alkaline lysis of transformed bacteria. The DNA quality and integrity were evaluated via electrophoresis in agarose gel 1 % (w/v) and the concentration was estimated by BioSpec-nano spectrophotometer (Shimadzu™) and via comparison in electrophoresis gel with samples at known concentrations. The DNA was diluted to 1000 ng/µL and 8 µL of each component were precipitated in tungsten particles with 1,25 M $CaCl_2$ and 15 mM spermidine, and washed with ethanol. Each preparation was distributed among 6 membranes to bombard the plants. Five plants from each genotype were mock-inoculated and 30 plants from each genotype were CabCLV-inoculated. All the plants were placed in the growth chamber at 22 ºC and photoperiod of 10 h light/ 14 h dark.

Samples of the youngest leaves were collected at 7, 14, 21 and 28 days after biolistic inoculation. The DNA was extracted and the viral infection was diagnosed via PCR with the degenerated primers PCRC1 and PBL2040 (Rojas *et al.*, 1993; table S1). Infected samples confirmed at 14 and 21 dpi (days-post infection) were quantified, diluted to 100 ng/µL and organized in six or seven pools of three or four samples to further quantify the viral DNA, as described by Zorzatto *et al.* (2015). The genomic units of the CabLCV component B were normalized to the internal control 18S rDNA. Standard curves based on the regression analysis of the Ct values of CabCLV B and 18S rDNA were deployed to calculate genomic units.

3.13 RT-qPCR

The extraction procedure of Arabidopsis RNA samples was performed using the Trizol reagent (Invitrogen™), followed by precipitation with isopropanol. The sample integrity was evaluated through electrophoresis in 1% agarose gel (w/v) and they were quantified by BioSpec-nano spectrophotometer (Shimadzu™). Around 5 µg of RNA were treated with DNase I, RNase-free (Thermo Fisher Scientific™) and 2 µg were used for cDNA synthesis using 1 U of M-MLV Reverse Transcriptase (Thermo Fisher Scientific™) and Oligo (dT)18 primer (0,5 µM).

For RT-qPCR analysis, approximately 20 ng of cDNA was used as template, along with specific primers and 5 µL SYBER™ Green PCR Master Mix (Thermo Fisher Scientific™), resulting in 10 µL per reaction. The RT-qPCR assays were carried out in a 7500 Real-Time PCR System thermocycler (Thermo Fisher Scientific) and the reactions were developed with 10 min at 94°C and 40 cycles of 94°C for 15 s and 60°C for 60 s. The *actin* gene was used as an endogenous normalizer for the analysis with *NIG* and *CSN5A* gene expression, whereas the *18S* gene was deployed as a control for the quantification of CabCLV B in the viral infection assays (Table S1).

4. RESULTS

4.1 Salicylic acid affects NIG localization and homeostasis

Here, we further demonstrated that NIG displays nucleocytoplasmic shuttling property by using leptomycin B (LMB), a specific inhibitor of the nuclear export signal (NES)-dependent transport. Under these conditions, the fluorescence signal of transiently expressed NIG fused to GFP was detected in the nucleus, indicating that the rapid nuclear export of NIG is sensitive to LMB (Supplementary Figure 1). Nevertheless, in the absence of the nuclear export inhibitor, NIG preferentially accumulates within the cytoplasmic compartment suggesting that the overall nuclear import rate may be limiting, or NIG nuclear export rate may be exceeding. These observations raised the possibility that other stimuli may promote regulated traffic of NIG to the nucleus. To address this issue, we next examined whether phytohormones, which have been shown to participate in signaling events associated with resistance against begomoviruses, would alter NIG localization and homeostasis to counteract its proviral function, similarly to the WWP1 antiviral mechanism.

To evaluate whether plant hormones also trigger the NIG cellular relocalization, roots fragments from the *A. thaliana* transgenic line Col-0/35S::NIG-GFP were incubated with SA, MeJA, ACC, 2,4-D and ABA solutions and the fluorescence signal of the fused protein was observed under a confocal microscope. SA treatment, but not MeJA, ACC, 2,4-D, and ABA treatments, increased the nucleus-localized NIG in stably transformed roots (Figure 1A). Because SA has also been shown to trigger protein degradation in the nucleus of transfected cells, we evaluated whether SA could also influence the NIG homeostasis.

A. thaliana Col-0/35S::NIG-GFP and *A. thaliana* Col-0/2x35S::NIG-HA lines (Supplementary Figure 2A) were treated with SA in media supplemented with the protein synthesis inhibitor cycloheximide (CHX) and the proteasome inhibitor MG132. After 9 hours of SA treatment, the fusion protein NIG-HA levels were decreased (Figure1B, Supplementary Figure 3A-B). Quantification of NIG-HA levels via ImageJ software demonstrated that the samples treated with SA displayed significantly reduced levels of NIG-HA after 9 and 12 hours of incubation (Figure 1C). The inclusion of proteasome inhibitor MG132 in SA-treated samples prevented the alteration in NIG-HA levels (Figure 1D-E, Supplementary Figure 3C-D). The MG132-treated samples did not present detectable NIG turnover rates, and SA induced significant changes

over time. Exchanging the NIG tag to GFP did not alter the results because SA also promoted degradation of NIG-GFP, which was inhibited by the inclusion of MG132 (Supplementary Figure 3E and 3F). Furthermore, SA induced NIG ubiquitination, as shown by the enhanced ubiquitination level of immunoprecipitated NIG-HA under SA treatment compared to control sample (Figure 1F, Supplementary Figure 5A).

We next examined both SA-induced NIG relocalization and turnover by nuclear fractionation. Seedlings from *A. thaliana* Col-0/35S::NIG-GFP and *A. thaliana* Col-0/35S::NIG-HA were exposed to SA and MG132 and then were subjected to nuclear fractionation. NIG-HA and NIG-GFP accumulated to a greater extent in the nuclear extracts of SA- and MG132-treated samples than in the nucleus of samples treated with MG132 (Figure 1G and Supplementary Figure 4C). The assay performed with Col-0/35S::NIG-GFP showed that NIG was not redirected to the nucleus due to either one stimulus or untreated-samples (Supplementary Figure 4C). Differences in loading and contamination between fractions were monitored by probing the cytoplasmic enzyme UGPase and the nuclear enzyme RNApolII with specific antibodies. In the subcellular fractionation, the resulting cytosolic fraction was highly diluted and had to be concentrated to detect cytosolic NIG (compare the top and second blot of Figure 1G). The detection of a higher accumulation of nuclear NIG was dependent on both SA and the MG132 proteasome inhibitor. The same experimental design was repeated independently three times for the Col-0/2x35S::NIG-HA genotype (Supplementary Figure 4A and 4B). The results confirmed that SA induces the NIG redistribution to the nucleus, where it is degraded via the proteasome.

SA has been shown to regulate the phosphorylation status of regulated trafficking proteins involved in immunity and development (Lee *et al.*, 2015; Tan *et al.*, 2020; Zhang *et al.*, 2020). To gain insights into the mechanism by which SA modulates NIG redistribution and turnover, we assayed NIG phosphorylation and ubiquitination as possible PTMs related to SA. The polyubiquitination pattern of immunoprecipitated NIG-HA was detected to high levels in the SA-treated seedlings and barely detected in control, untreated seedlings (Figure 1F, Supplementary Figure 5A). In contrast, NIG phosphorylation signals corresponding to threonine, serine, and tyrosine phosphosites were detected to the same extent in SA-treated samples and control samples (Supplementary Figure 5B). Although these results may indicate that SA-induced phosphorylation may not be the trigger for SA-mediated NIG redistribution, they do not

exclude the possibility that differential phosphorylation at specific residues may account for the relocation of NIG to the nucleus.

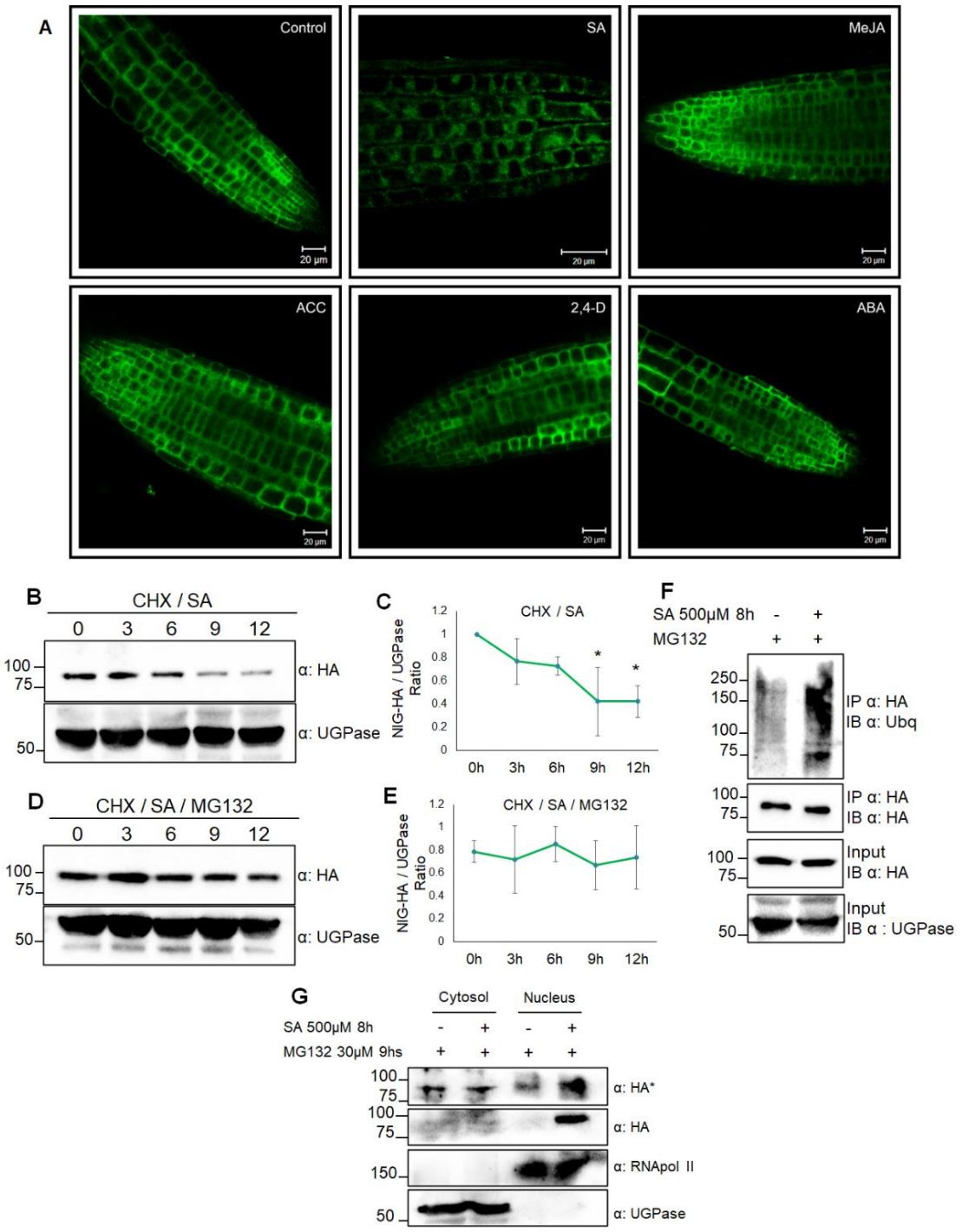

Figure 1. Salicylic acid induces NIG nuclear relocation and degradation.

A. The hormone SA, but not ABA, ACC, MeJA and 2,4-D, redirects NIG to the nucleus, as displayed by confocal fluorescence image of Col0/35S:NIG-GFP root cells. **B.** NIG-HA is degraded after 9 h of SA 500 µM treatment. NIG-HA expressing seedlings were treated with SA and protein accumulation was monitored by immunoblotting NIG-HA with anti-HA. **C.** In NIG turnover assays, the immunoblotting signals corresponding to NIG-GA bands were quantified using the Image-J software from Biorad. The data was normalized to the signal of UGPase, an endogenous control (J<0.05, n=3). **D.** The proteasome inhibitor MG132 30 µM prevents SA-mediated NIG-HA degradation. **E.** The same calculation did in **C** was performed**.** Col0/2x35S::NIG-HA plants were utilized and the protein synthesis inhibitor cycloheximide (CHX) 100 µM was included in all samples of **B,C,D** and **E** experiments. **F.** NIG-HA is polyubiquitinated upon SA treatment. Col0/2x35S::NIG-HA plants were utilized. **G.** NIG-HA level increase in the nuclear fraction upon SA treatment. Col0/2x35S::NIG-HA plants were utilized. The "*" corresponds to samples with concentrated cytosol. For all nuclear fractionation assay, the cytosolic protein UGPase and the nuclear protein RNApolII were utilized as endogenous controls for loading and contamination control between fractions.

Because WWP1 has been shown to drive NIG translocation to the nucleus, we next examined whether the SA-mediated NIG redistribution would require a WWP1-dependent active transport mechanism. This hypothesis was tested by first transforming the *atwwp1-1* mutant line with a DNA construct expressing YFP-NIG (Supplementary Figure 2B) and then accessing the localization of the fused protein in the presence and absence of SA by confocal microscopy and nuclear fractionation. Fragments of *atwwp1*/YFP-NIG roots were treated with SA, and the fluorescence of the YFP-NIG was also identified in the nucleus, although to a low frequency, which may be due to SA-mediated degradation of nuclear YFP-NIG (Figure 2A). Inclusion of MG132 in the fractionation assay prevented proteasome-mediated turnover of nuclear NIG, demonstrating that AtWWP1 does not influence the SA-mediated NIG relocation. (Figure 2B).

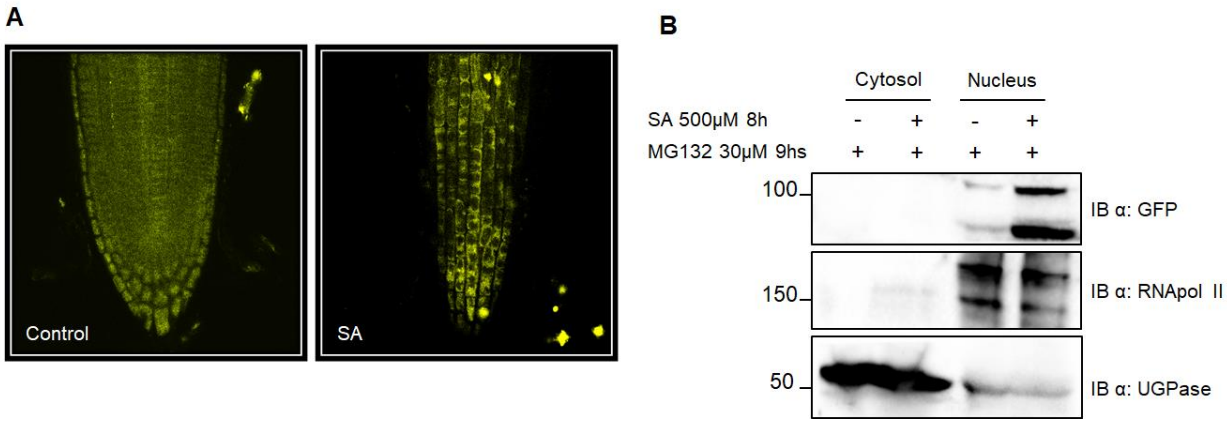

Figure 2. AtWWP1 does not influence the SA-mediated NIG relocation.

A. YFP-NIG is relocated to the nucleus due to SA 500 µM 6h treatment, as displayed by confocal fluorescence image of *Atwwp1*/YFP-NIG root cells. **B.** YFP-NIG levels increase in the nucleus due to SA in nuclear fractionation assay. The cytosolic protein UGPase and the nuclear protein RNApolII were utilized as endogenous controls for loading and contamination between fractions. The *atwwp1*/35S::YFP-NIG line 2 was deployed.

4.2 NIG turnover is induced by its partner CSN5A

Machado (2011) identified that the COP9 signalosome complex subunit 5a (CSN5A) could interact with NIG via yeast two-hybrid assay, Co-IP performed in *N. benthamiana*, and BiFC in the onion root cells. Confocal microscopy of *N. benthamiana* leaves co-infiltrated with YFP-NIG, and CSN5A-GFP demonstrated that a small fraction of both fusion proteins colocalized in the nucleus (Machado, 2011). This reduced colocalization led to the interpretation that CSN5A interaction could trigger NIG relocation to the nucleus. Although the data on CSN5A-NIG dynamic identified

that the complex was formed in the nucleus of a small fraction of onion root cells, the NIG-CSN5A complex formation was not verified in any cellular compartments in the model plant *N. benthamiana*. Additionally, the Co-IP results failed to show the input controls, an unrelated protein as a negative control, in addition to having been restricted to the immunoprecipitation of a single protein from the complex; the reverse experiment was not performed. To better address these issues, new assays were conducted.

As a subunit of the COP9 signalosome complex, CSN5A could potentially regulate the NIG proteolysis. We next examined whether the NIG stability could be affected by transiently co-expressing CSN5A in *N. benthamiana* leaves. NIG-HA accumulated stably when transiently expressed alone or combined with the unrelated GFP protein but was barely detected when co-expressed with CSN5A (Supplementary Figure 6A). This result may be due to CSN5A-induced proteasome-mediated degradation of NIG because the inclusion of 50 μM MG132 for 12 h increased NIG accumulation to detectable levels (Supplementary Figure 6B). The treatment with 100 μM MG132 for 18 hours prior to harvesting the infiltrated leaves transiently expressing NIG and CSN5A was very effective in preventing the negative role of CSN5A upon NIG homeostasis (Supplementary Figure 6C).

The *in vivo* interaction between NIG and CSN5A was then confirmed by BiFC assay (Figure 3A and 3B). *N. benthamiana* leaves co-infiltrated with *A. tumefaciens* harboring NIG and CSN5A fused to the complementary halves of YFP were imaged via confocal microscopy 48 hours after infiltration. In the absence of MG132, NIG and CSN5A interaction was only observed with the NIG-SPYCE and CSN5A-SPYNE combination (Figure 3A). The additional treatment of MG132 enabled the reconstruction of the yellow fluorescent protein (YFP) signal by NIG-SPYNE/CSN5A-SPYCE complex (Figure 3B). For both constructs, the reconstructed YFP signal was observed only in the cytoplasm. Control combinations were also performed (Supplementary Figure 7A and 7B).

In vivo interactions between NIG and CSN5A were also monitored by co-immunoprecipitation assays. Full-length NIG-GFP and CSN5A-HA fusions were transiently co-expressed in *N. benthamiana* leaves. Controls by expressing the fusion protein alone and the unrelated protein eGFP were also included. MG132 100 μM was infiltrated 18 hours before harvesting the sample. Anti-GFP magnetic beads directly immunoprecipitated NIG-GFP, but not CSN5A-HA, from protein extracts of co-

infiltrated leaves, confirming the specificity of the antibody. Nevertheless, the anti-GFP-immunoprecipitated complex also contained CSN5A-HA as shown by the Co-IP blot probed with anti-HA, indicating a previous association between NIG-GFP and CSN5A-HA. The Co-IP results also demonstrated that GFP alone did not interact with CSN5A, demonstrating the specificity of the interactions between NIG and CSN5A. Switching the protein tags did not alter the results because CSN5A-GFP, but not GFP alone, was also associated with NIG-HA in infiltrated extracts (Figure 3D).

To address the NIG-CSN5A interaction *in planta*, an additional Co-IP assay was designed using transgenic lines expressing NIG-HA. Using anti-CSN5A serum, endogenous CSN5A was detected in the NIG-HA immunoprecipitated complex from both SA/MG132-treated extracts and MG132-treated samples (Figure 3E). Immunoblotted UGPase protein was used as loading controls. Anti-HA-immunoprecipitated complexes from Col-0 extracts were used as negative controls.

Here, we showed that overexpression of CSN5A decreases susceptibility to the begomovirus CabLCV (Supplementary Figure 8). CSN5A-overexpressing lines (Supplementary Figure 8A and 8B) displayed attenuated symptoms and accumulated lower vDNA compared to Col-0-infected plants (Supplementary Figure 8C and 8D).

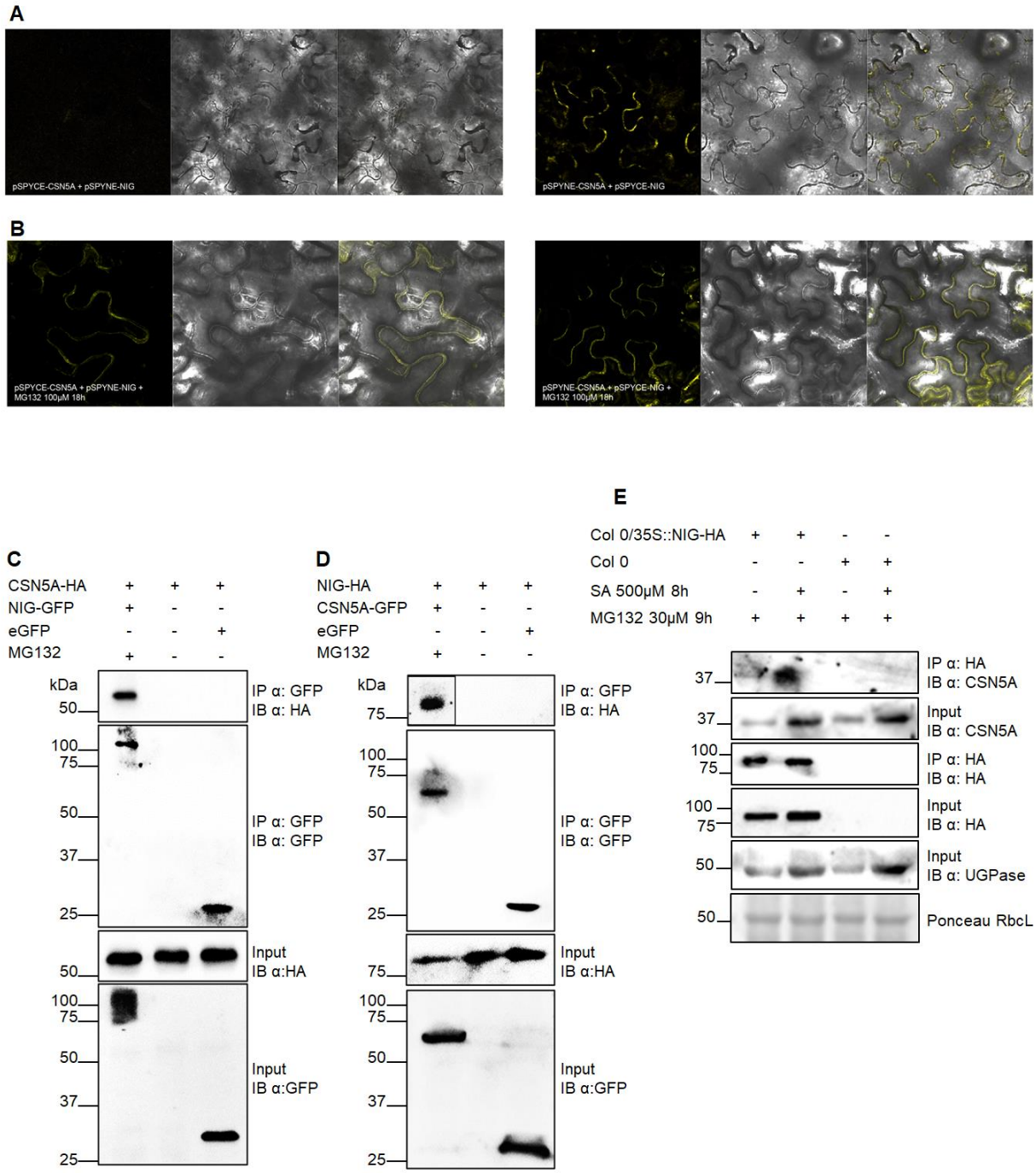

Figure 3. NIG interacts with CSN5A.

A-B. *In vivo* interaction between NIG and CSN5A by bimolecular fluorescence complementation (BiFC) analysis. The interaction of NIG-SPYCE and CSN5A-SPYNE combination was only observed in samples pre-treated with MG132 100 μM 18h. The YFP fluorescence was evaluated in *Nicotiana benthamiana* leaves co-infiltrated with 35S::NIG-SPYNE + 35S::CSN5A-SPYCE and 35S::NIG-SPYCE + 35S::CSN5A-SPYNE fusion proteins. **C-D.** NIG and CSN5A co-immunoprecipitation (Co-IP) assay. The indicated constructs were expressed in *Nicotiana benthamiana* leaves and the immunoprecipitation assays was performed with anti-GFP magnetic beads. In **D**, the bar indicates combined samples from two independent experiments. **E.** NIG and CSN5A co-immunoprecipitation (Co-IP) in plants with and without SA treatment. Col0/35S::NIG-HA plants were used and the immunoprecipitation was performed with anti-HA magnetic beads. For CSN5A, an anti-CSN5A was used. The protein UGPase was utilized as endogenous control for loading.

4.3 Loss-of-NIG function does not enhance resistance against begomovirus

NIG has been described as a positive contributor to begomoviral infection based on two significant pieces of evidence (Carvalho *et al.* 2008a). Firstly, NIG binds *in vivo* with NSP and may accessorize the NSP traffic from the nucleus to the cytosol. Secondly, NIG overexpression in *A. thaliana* transgenic lines enhances susceptibility to CabLCV. Nonetheless, studies comparing Col0, *atnig-1* null mutants, and complemented *atnig* lines are still needed to further examine the NIG proviral function. For that purpose, the *atnig-1* T-DNA insertional mutant was requested from the ABRC (SALK_014974) and transformed with the 35S::YFP-NIG constructs.

Three independently complemented lines were selected for the infectivity assay (Figure 4A). The Col0, *atnig-1* null mutants, and complemented *atnig-1* lines were challenged against the begomovirus CabCLV DNA-A and DNA-B by biolistic delivery. The course of infection was monitored as described by Florentino *et al.* (2006). The symptoms and vDNA accumulation were also evaluated. The phenotypes of mock inoculated lines were visibly indistinguishable from Col-0 (Supplementary Figure 10). The infection rates and viral DNA accumulation for 14 days post infection (d.p.i) and 21 d.p.i did not display significant differences between any of the genotypes (Figure 4B-4D). Likewise, the disease symptoms did not differ among the infected genotypes (Supplementary Figures 9). Not consistently with the current infection results displayed by *atnig-1* mutant line, NIG overexpression has been previously shown to enhance the susceptibility of transformed lines to begomoviruses (Carvalho *et al*., 2008a). Either *atnig-1* is a weak mutant allele or functional redundancy of the NIG most related genes may explain these apparent controversial results.

.

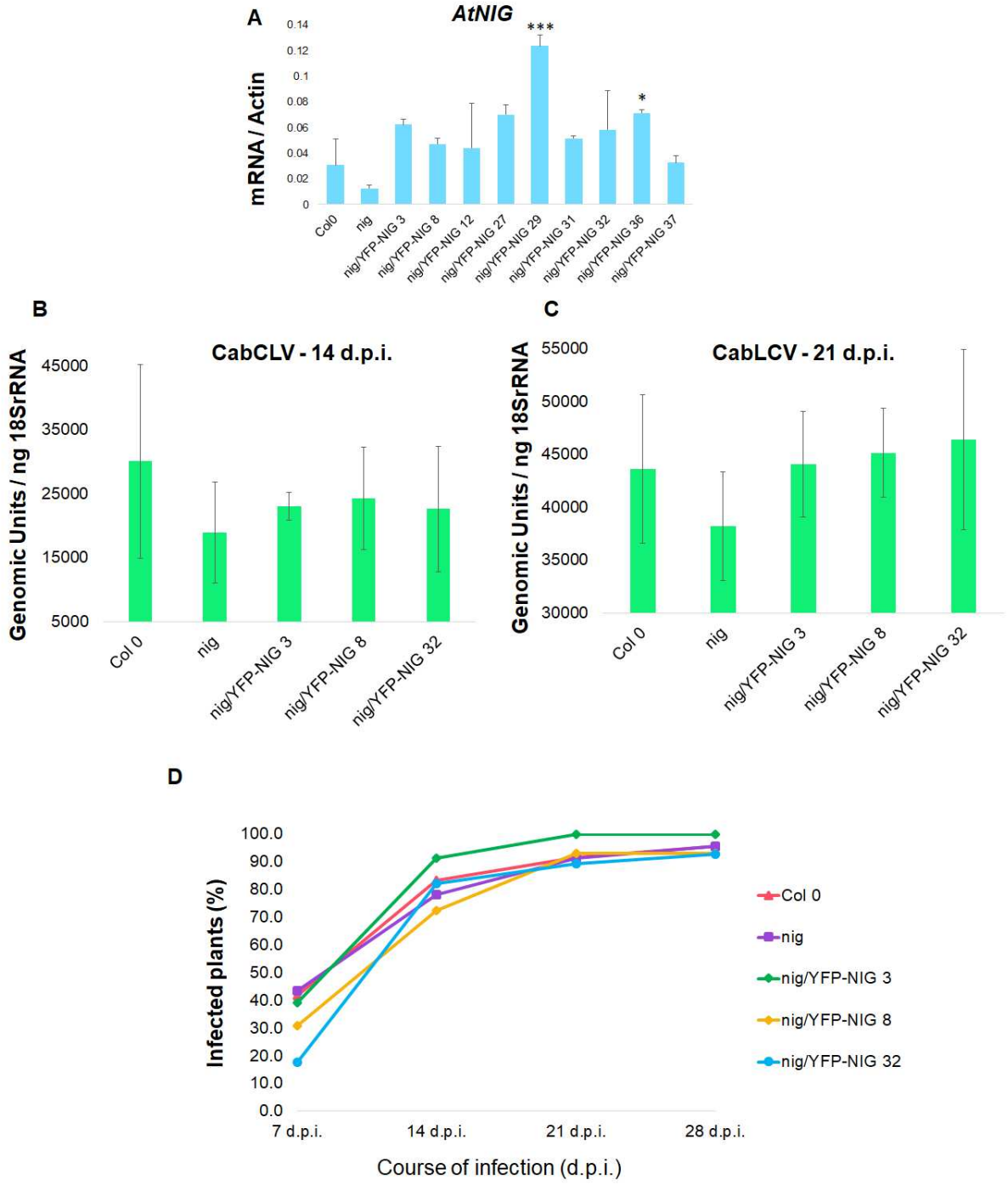

Figure 4. Loss-of-NIG function does not affect CabLCV infection.

A. Transcript accumulation of AtNIG transcript in Col0, *atnig* and 9 transgenic complemented lines (*Atnig*/YFP-NIG). The levels of *AtNIG* transcript were determined by RT-qPCR using actin as an endogenous control. The asterisks indicate statistically significant differences by the test-t (*p<0.05, ***p<0.001). **B-C.** Col-0, *nig* and 3 *nig*/YFP-NIG independent lines were challenged against begomovirus CabCLV via biolistics. vDNA accumulation was determined by qPCR at 14d.p.i. (B) and 21 d.p.i (C). The 18S ribosomal RNA was used as template for normalization. **D.** Progression of infection in Col-0, *nig* and 3 *nig*/YFP-NIG independent lines. Values represent viral infected plants confirmed by PCR.

5. DISCUSSION

The movement proteins from begomoviruses play a crucial role in accessorizing the viral traffic from the nucleoplasm, where new vDNA is synthesized, to the cytoplasm and then to the adjacent cells via plasmodesmata (Gafni and Epel, 2002; Rojas *et al.*, 2018). This coordinated transport by NSP and MP proteins is indispensable to viral spread, and deciphering this process relies on the research in host-virus protein-protein interactions. NSP deviates several host proteins from their ordinary function in different cellular compartments to ensure viral success (Martins *et al.*, 2020). For example, NSP modulates the host physiology by inhibiting protein functions, including the kinase domain inhibition of the transmembrane receptor NIK1 A-loop (Fontes *et al.*, 2004; Mariano *et al.*, 2004) and the steric disabling of the acetylase NSI oligomers (Carvalho *et al.*, 2006). Furthermore, NSP modulates the transcription level of host genes by upregulating the proviral *AS2* or downregulating terpene biosynthesis genes (Ye *et al.*, 2015; Li *et al.*, 2014). As a facilitator of intracellular movement of vDNA, NSP also recruits host transport functions, co-opting the intracellular transport proteins NIG and NISP to mediate vDNA trafficking (Carvalho *et al.* 2008a; Gouveia-Mageste *et al.* 2021). Each component of the NSP-derived immune hub exhibits functional peculiarities that require specific approaches to establish accurate mechanistic models to elucidate their roles.

The previously studied GTPase, NIG, in consonance with NISP paves a path to vDNA-NSP transport along the cytosol and helps the vDNA-NSP-MP association in endosomes and further exportation of vDNA to adjacent cells (Gouveia-Mageste *et al.*, 2021). Antagonistically, WWP1 subverts the NIG shuttle propriety by entrapping it in the nucleus (Calil *et al.*, 2018). Given the NIG partners dynamic, it is feasible to assume that processes that reallocate NIG from the cytosol may constitute antiviral responses, while mechanisms that exploit its cytosolic perinuclear disposition might lead to proviral roles.

5.1 SA regulates NIG degradation and relocation to the nucleus.

Confocal microscopy of *A.thaliana* roots stably expressing the fusion protein NIG-GFP provided evidence that SA alters the NIG subcellular distribution to the nucleus, which was further confirmed by fractionation assays (Figure 1A, 1G and Supplementary Figure 4). In addition to redirecting NIG from the cytosol to the nucleus, SA induces NIG ubiquitination and negatively modulates NIG homeostasis, a condition

that may be prevalent during viral infection and increase SA levels (Figure 1B-1F and Supplementary Figures 3 and 5A). Although SA increases the NIG nuclear levels, our data showed that steady-state SA concentrations are sufficient to maintain basal NIG levels in the nucleus. This SA-triggered subcellular redistribution of NIG is independent of WWP1-mediated nuclear transport mechanisms, a cellular factor that also mediates NIG redirection to the nucleus (Figure 2).

As a crucial hormone in plant immunity, SA levels is associated with a wide range of local and systemic responses against biotrophic and semi-biotrophic pathogens (Qi *et al.*, 2018; Zhang and Li, 2019). SA is induced by and participates in PAMP triggered immunity (PTI) and Effector Triggered Immunity (ETI) signaling events and is also crucial to systemic acquired resistance (SAR) activation in distal tissues (Bonardi *et al.*, 2011; Durrant and Dong, 2004; Gaffney *et al.*, 1993; Kong *et al.*, 2016; Terrence *et al.*, 1994; Wiermer *et al.*, 2005). The SA methylated form, MethylSalicylate (MeSA), can also serve as a SAR eliciting signal between neighbor plants. Consistently with SA central relevance in plant immunity, pathogens often develop mechanisms to subvert the defense responses associated with SAR. The defense strategies include the conversion of SA to inactive forms, the impairment of SA biosynthesis, and the interference with SA signaling (Qi *et al.*, 2018).

Among SA-related proteins, NPR1 is a key regulator of SA levels (Spoel *et al.*, 2003; Lai *et al.*, 2018). Upon SAR, NPR1 dissociates from its homo-oligomeric complexes, via thioredoxin-mediated dissulfide bonding breakage to its monomeric configuration, which translocates to the nucleus where it is polyubiquitinated, degraded via ubiquitin proteasome system (UPS), phosphorylated, and acts as co-activator of defense genes (Spoel *et al.*, 2009; Zhang *et al.*, 2020; Zavaliev *et al.*, 2020). Our current results demonstrated that NIG shares some similarities with NPR1 concerning SA-mediated degradation and regulated traffic to the nucleus (Figure 1 and 2). However, NIG and NPR1 apparently diverge on their SA-induced posttranslational modification status because the phosphorylation profile of NIG does not change after SA treatment. By immunoblotting immunoprecipitated NIG-HA with anti-phospho amino acid antibodies, we showed that NIG was phosphorylated in serine, threonine, and tyrosine residues under normal conditions and after SA treatment (Supplementary Figure 5B). Phosphoproteomic analysis revealed that NIG seems to be phosphorylated under normal conditions (Jones, A., personal communication). However, treatment with flg22, the active peptide of the flagellin PAMP, promotes differential

phosphorylation of NIG, and only a Ser at position 164 remains highly phosphorylated (Jones, A., personal communication). Flg22 is a stimulus recognized by the PAMP recognition receptor (PRR) FLS2 and constitutes an essential signal that induces posttranslational modifications in many defense proteins. For example, the coreceptor Botrytis Induced Kinase 1 (BIK1) is phosphorylated by the receptor FLS2 after flg22 perception. Then, BIK1 undergoes flg22-mediated PTMs such as monoubiquitination and phosphorylation to participate in immunity signal transduction (Ma *et al.*, 2020; Lu *et al.*, 2010). The flg22-mediated phosphorylation of NIG points to a new mechanism that could also control the NIG function.

Albeit NIG is relocated and then degraded upon SA, it is still unclear whether the protein turnover happens in the nucleus. Additional experiments may elucidate whether NIG is sent to the nucleoplasm to be degraded or whether SA induces NIG turnover in the cytosol while increasing its nuclear traffic. Nevertheless, we provided several lines of evidence that support the first alternative. First, our fractionation assay demonstrated that MG132 enhanced the accumulation of NIG in the nucleus but did not change the levels of NIG in the cytosol. Second, ubiquitinated NIG was detected in the SA-treated protein extract. Finally, NIG interacted with the COP9 signalosome subunit CSN5A, which oligomerizes with the COP9 signalosome subunits to mediate proteosome-dependent degradation of proteins in the nucleus (Kwok *et al.*, 1998; Wei *et al.*, 2008; Jin *et al.*, 2014). The NPR1 mechanistic model may shed light on possible experimental approaches to address the NIG nucleocytoplasmic dynamic and the discovery of eventual partners and functional modulators. Additionally, in the Arabidopsis Interactome-1 (AI-1), several *A.* thaliana protein-protein interactions were discovered via yeast two-hybrid assay (Yazaki *et al.*, 2016). One of this interactome branches, the NAPPA network, identified putative interactions between 38 transcription factors, from which NIG has been demonstrated to interact with AtbZIP53 (AT3G62420), AtbZIP63 (AT5G28770), ABI5 (AT2G36270), and HAT22 (AT4G37790). Interestingly, AtbZIP53, AtbZIP63, and ABI5 have also been shown to interact with NPR1 by the NAPPA database (Yazaki *et al.*, 2016).

5.2 CSN5A is a negative modulator of NIG activity.

The protein CSN5A is one of the eight subunits that compose the nuclear oligomeric complex of the signalosome. The signalosome presents two MPN domain-containing subunits, CSN5 and CSN6; and six PCI or PINT domain-containing

subunits, the CSN1, CSN2, CSN3, CSN4, CSN7, and CSN8 subunits (Wei and Deng, 2003). Unlike CSN6, CSN5 exhibits isopeptidase activity responsible for deneddynilation of cullins (Cope *et al.,* 2002; Maytal-Kivity *et al.,* 2002). The CSN complex shares similarities with the 26S proteasome lid, including the stoichiometry of 2 MPN: 6 PCI subunits and the active MPN+ catalytic subunit, represented by CSN5 in the signalosome and by Rpn11 in the proteasome (Verma *et al.*, 2002; Maytal-Kivity *et al.*, 2002). CSN5A, or its paralog CSN5B, dennedylation activity is activated on the holo-complex composition, but CSN5A also occurs as cytosolic monomers, which may display additional functions apart from cleaving Nedd8 from cullins (Schwechheimer and Isono 2010).

CSN5A has been characterized as a relevant immune hub due to convergent interactions of several host defense proteins and different effectors from divergent pathogens (Mukhtar *et al.*, 2011). Among the CSN5A-interacting effectors, L2/C2 from geminiviruses has been shown to interact with and inhibit the activity of CSN5A (Lozano-Durán *et al.*, 2011). The mutant *CSN5A* have been shown to be more susceptible to the geminivirus *Beet Curly Top Virus* (BCTV) (Lozano-Durán and Rodríguez-Bejarano, 2011).

The results of this investigation indicate that CSN5A negatively regulates the NIG stability, which can be recovered even in the presence of CSN5A overexpression by inhibiting the proteasome activity (Supplementary Figure 6). Accordingly, CSN5A interacts with NIG in the cytosol, and MG132 enables the complex pSPYCE-CSN5A/pSPYNE-NIG formation. Although we did not detect the complex in the nucleus even in the presence of MG132, the nuclear redistribution of the CSN5A-NIG complex may be SA-dependent because we demonstrated that SA induces the nuclear redistribution and turnover of NIG. SA has also been demonstrated to enhance the affinity between NPR1 and CSN5A and E3 ligases, leading to increased degradation rates of NPR1 by the ubiquitin-proteasome pathway (Spoel *et al.* 2009). It is also reasonable to predict that the SA-mediated degradation of NIG is dependent on CSN5A regulatory activity. The SA-increased NIG pool in the nucleus may favor the interaction between NIG and CSN5A in its oligomeric configuration, in which CSN5A exhibits its proteolytic activity. Moreover, this nuclear increase of NIG might be an ideal control treatment in future attempts to visualize the NIG-CSN5A complex formation in *N. benthamiana* nucleus through BiFC.

By overexpressing NIG and CSN5A transiently in *N. benthamiana*, Machado (2011) detected nuclear co-localization of NIG and CSN5A in a small fraction of cells, a result that may indicate a temporary transition due to the nuclear degradation of NIG. However, since the YFP and GFP tags fused to these proteins present similar wavelengths, it is necessary to evaluate the same experiment as Machado (2011) with other fluorescent tag combinations, such as mCherry and GFP. Moreover, the CSN5A-mediated degradation of proteins depends on the COP9 signalosome eight-subunit (CSN1–8) protein complex that controls protein ubiquitination by deneddylating Cullin-RING E3 ligases (CRLs) in the nucleus. Based on the results of this investigation and other previously published results, we propose that NIG interacts with CSN5A in the cytosol under normal conditions. Begomovirus infection induces the accumulation of SA that in turn mediates the translocation of the NIG-CSN5A complex to the nucleus, where it is degraded via the proteasome. Alternatively, the SA-induced nuclear NIG interacts with the COP9 signalosome complex via CSN5A in the nucleus where CSN5A denneddynilates yet-to-be-identified E3 ligases that recognize NIG as a substrate, resulting in NIG polyubiquitination and proteolysis by the UPS pathway (Figure 5). This model predicts that the SA-mediated nuclear relocalization and turnover of NIG may be an antiviral defense strategy of plant cells to prevent the NIG proviral function, that otherwise would facilitate the transport of vDNA to the cytosol favoring infection.

A recent study that performed BiFC to verify the interaction between CSN5A and the Microtubule-associated protein SPR1 and the bZIP transfactor HY5 successfully visualized CSN5A-SPR1 complex formation in the nucleus and cytosol and the CSN5A-HY5 interaction in the nucleus (Xiaoxia *et al.*, 2019). No proteasome or degradation inhibitors were utilized to observe the CSN5A-HY5 and CSN5A-SPR1 interactions via the BiFC system (Xiaoxia *et al.*, 2019). Mir and León (2014) detected via BiFC that the membrane-localized PCC1 could recruit CSN5A and CSN5B to the plasma membrane, which was associated with an additional PCC1 regulation step that would rely on CSN5A activity, but that would differ from that observed in CSN holo-complexes.

Conversely, another explanation for the impossibility of visualizing nuclear CSN5A-NIG complex formation is the steric hindrance between the amino- and carboxyl-terminal portions of YFP protein with the COP9 components. Accordingly, the cytosol-localized and monomeric CSN5A did not display the same hindrance that enables the interaction with its partners. In addition, the YFP fluorescence pSPYCE-

CSN5A/pSPYNE-NIG was only restored when 100 µM MG132 was applied (Figure 3A-B). The MG132 treatment could also favor the YFP restoration due to the NIG proteolysis inhibition and consequent increase in the NIG pool. The configuration pSPYCE-CSN5A/pSPYNE-NIG could also structurally favor degradation over the combination pSPYCE-NIG/pSPYNE-CSN5A; thereby, MG132 would favor sufficient NIG levels to detect the interactions via BiFC. Additional studies are necessary to fully understand the effects of the SA stimuli and CSN5A interaction on NIG homeostasis and function.

5.3 NIG null mutant does not increase resistance to begomovirus

A proviral function was assigned to NIG based on the observation that *NIG* overexpression in Arabidopsis led to enhanced susceptibility to begomovirus infections and the NIG ability to facilitate the vDNA-NSP nuclear export to the cytosol (Carvalho *et al.*, 2008a). In this investigation, we showed that, although the *atnig*/NIG complemented lines displayed equivalent viral accumulation and infection rates as Col-0, the null mutant *atnig-1* was ineffective in providing reduced infection rates and depleted viral accumulation to Col-0 (Figure 4B-D). The viral accumulation in the knockout leaves was lower than Col-0, although the average of two independent biological replicates was not statistically significant at $p<0.05$. This trend may assign the *atnig-1* mutant as a weak allele of a susceptibility gene that would depend on the concentration of the vDNA inoculum for significant effects on resistance. Accordingly, previous results from two independent experiments in the lab demonstrated a significant reduction in viral load in the *atnig-1* null alleles. Furthermore, NIG belongs to a small gene family, and other family members may function redundantly in begomovirus infection. Based on sequence alignment, NIG is related to At1g08680 and At4g32630, which share 75 and 71,4% identity within the ArfGAP domain and could mimic the NIG transport features. Although the interaction between the NIG paralogs and viral NSP from CabLCV has not been investigated, unpublished results from our lab have demonstrated that the four NIG paralogs from cassava interacts with NSPs from two species of *African Cassava Mosaic Virus* and also from CabLCV. These results demonstrate that the interaction NIG-NSP is conserved among different NIG paralogs of different plant species and NSPs from different begomoviruses. Therefore, biochemical analysis of the NIG functional modulators from different plant

species and NIG paralogs and NIG double and triple null mutants may better address this issue.

Alternatively, during begomovirus infections, increased SA levels could negatively affect NIG cytosolic pool and NIG accumulation, thus compromising the NIG-mediated transport of vDNA-NSP complexes. Concomitantly, the endogenous CSN5A would also contribute to subverting the NIG localization from the cytosol to the nucleus and also participating in the regulation of NIG levels. Therefore, the SA and CSN5A adverse effects on NIG turnover and the NIG strategic perinuclear localization would be sufficient to emulate the phenotype exhibited by Col-0 and *atnig*/NIG to that of *atnig-1*.

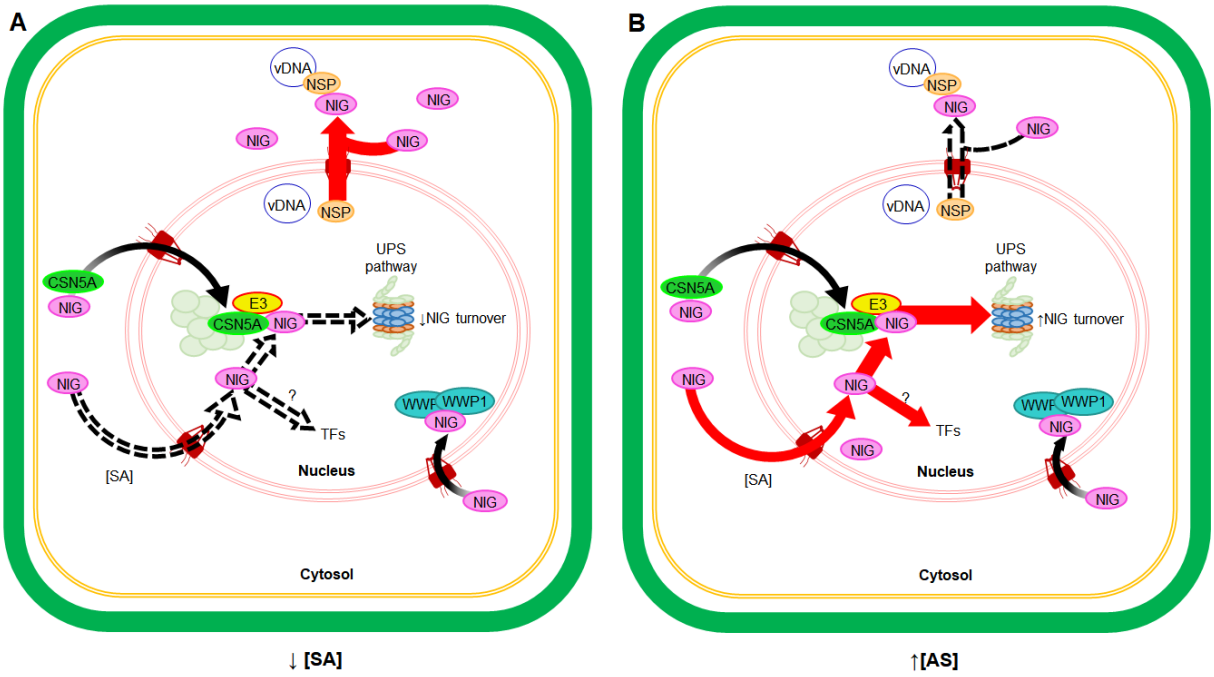

Figure 5. A mechanistic model of NIG regulation by SA and CSN5A.

A. Under steady-state conditions, NIG presents low pools in the nucleus and accumulates around the nuclear envelope, where NIG accessorizes NSP-vDNA nucleocytoplasmic transport. **B.** Stimuli such as viral infection and exogenous SA treatments lead to the intracellular increase of SA levels, thus inducing NIG turnover and translocation to the nucleus, which compromises the NIG role in NSP nuclear export. Additionally, an increased NIG nuclear pool may favor the NIG-CSN5A interaction and putative interaction with unidentified NIG targets like TFs and E3 ligases. In both scenarios, CSN5A acts as a nuclear import factor to NIG and regulates the NIG UPS-mediated degradation. The SA-induced nuclear translocation of NIG is not dependent on a WWP1-mediated active transport. Black discontinuous arrows indicated compromised functions. Red straight arrows indicated enhanced functions. Black continuous arrows: undefined functions.

6. CONCLUSIONS

In this investigation, we presented pieces of evidence on mechanisms that strategically modulate NIG, a GTPase that interacts with NSP and facilitates the transport of vDNA-NSP complex into the cytosol. First, we showed that SA mediated the NIG trafficking to the nucleus and degradation mediated by the UPS pathway. This SA influence is apparently independent of the WWP1-mediated nuclear import of NIG.

We also showed that CSN5A interacts with NIG *in vivo* and can induce NIG degradation, probably within the nucleus, where the COP9 signalosome complex is active for proteolysis. Furthermore, the proteasome inhibitor MG132 enhanced the NIG pools in the nucleus, consistent with the existence of a NIG-nuclear degradation mechanism. Our results implicated CSN5A as a component of the NIG-protein interaction hub, which is possibly responsible for negatively regulating NIG homeostasis and nuclear redistribution. Possibly, CSN5A- and SA-mediated degradation and nuclear relocation are part of the same coordinated process. It is feasible to assume that elevated SA levels by begomovirus infection negatively impact NIG pools and increase its nuclear import, reducing the NIG normal levels in the cytosol and mediating the NIG degradation in the nucleus. Based on these results, we propose that the SA-mediated nuclear reallocation that negatively regulates NIG turnover and cytosolic pools may be an evolutionary plant defense strategy to counteract the NIG proviral function. In contrast to what is predicted by the current model, the inactivation of the *NIG* gene in the *atnig-1* mutant line did not affect begomovirus infection. However, these results may be explained by the existence of closely related NIG paralogs in the Arabidopsis genome, which may function redundantly in begomovirus infection, or by the *atnig-1* mutant ineffectiveness.

REFERENCES

Alber, F., Dokudovskaya, S., Veenhoff, L. M., Zhang, W., Kipper, J., Devos, D., Suprapto, A., Karni-Schmidt, O., Williams, R., Chait, B. T., Sali, A., & Rout, M. P. (2007). The molecular architecture of the nuclear pore complex. *Nature*, *450*(7170), 695–701. doi: 10.1038/nature06405

Bonardi, V., Tang, S., Stallmann, A., Roberts, M., Cherkis, K., & Dangl, J. L. (2011). Expanded functions for a family of plant intracellular immune receptors beyond specific recognition of pathogen effectors. *Proceedings of the National Academy of Sciences of the United States of America*, *108*(39), 16463–16468. doi: 10.1073/pnas.1113726108

Calil, I. P., Quadros, I. P. S., Araújo, T. C., Duarte, C. E. M., Gouveia-Mageste, B. C., Silva, J. C. F., Brustolini, O. J. B., Teixeira, R. M., Oliveira, C. N., Milagres, R. W. M. M., Martins, G. S., Chory, J., Reis, P. A. B., Machado, J. P. B., & Fontes, E. P. B. (2018). A WW Domain-Containing Protein Forms Immune Nuclear Bodies against Begomoviruses. *Molecular Plant*, *11*(12), 1449–1465. doi: 10.1016/j.molp.2018.09.009

Carvalho, C. M., Fontenelle, M. R., Florentino, L. H., Santos, A. A., Zerbini, F. M., & Fontes, E. P. B. (2008a). A novel nucleocytoplasmic traffic GTPase identified as a functional target of the bipartite geminivirus nuclear shuttle protein. *Plant Journal*, *55*(5), 869–880. doi: 10.1111/j.1365-313X.2008.03556.x

Carvalho, C. M., Machado, J. P. B., Zerbini, F. M., & Fontes, E. P. B. (2008b). NSP-interacting GTPase: A cytosolic protein as cofactor for nuclear shuttle proteins. *Plant Signaling and Behavior*, *3*(9), 752–754. doi: 10.4161/psb.3.9.6641

Carvalho, C. M., Santos, A. A., Pires, S. R., Rocha, C. S., Saraiva, D. I., Machado, J. P. B., Mattos, E. C., Fietto, L. G., & Fontes, E. P. B. (2008c). Regulated nuclear trafficking of rpL10A mediated by NIK1 represents a defense strategy of plant cells against virus. *PLoS Pathogens*, *4*(12). doi: 10.1371/journal.ppat.1000247

Carvalho, M. F., Turgeon, R., & Lazarowitz, S. G. (2006). The geminivirus nuclear shuttle protein NSP inhibits the activity of AtNSI, a vascular-expressed arabidopsis acetyltransferase regulated with the sink-to-source transition. *Plant Physiology*, *140*(4), 1317–1330. doi: 10.1104/pp.105.075556

Carvalho, M. F., & Lazarowitz, S. G. (2004). Interaction of the Movement Protein NSP and the Arabidopsis Acetyltransferase AtNSI Is Necessary for Cabbage Leaf Curl

Geminivirus Infection and Pathogenicity. *Journal of Virology*, *78*(20), 11161–11171. doi: 10.1128/jvi.78.20.11161-11171.2004

Cavazza, T., & Vernos, I. (2016). The RanGTP pathway: From nucleo-cytoplasmic transport to spindle assembly and beyond. *Frontiers in Cell and Developmental Biology*, *3*(82). doi: 10.3389/fcell.2015.00082

Chavrier, P., & Goud, B. (1999). The role of ARF and Rab GTPases in membrane transport. *Current Opinion in Cell Biology*, *11*(4), 466–475. doi: 10.1016/S0955-0674(99)80067-2

Chen, F., D'Auria, J. C., Tholl, D., Ross, J. R., Gershenzon, J., Noel, J. P., & Pichersky, E. (2003). An Arabidopsis thaliana gene for methylsalicylate biosynthesis, identified by a biochemical genomics approach, has a role in defense. *Plant Journal*, *36*(5), 577–588. doi: 10.1046/j.1365-313X.2003.01902.x

Chinchilla, D., Zipfel, C., Robatzek, S., Kemmerling, B., Nürnberger, T., Jones, J. D. G., Felix, G., & Boller, T. (2007). A flagellin-induced complex of the receptor FLS2 and BAK1 initiates plant defence. *Nature*, *448*(7152), 497–500. doi: 10.1038/nature05999

Christie, M., Chang, C. W., Róna, G., Smith, K. M., Stewart, A. G., Takeda, A. A. S., Fontes, M. R. M., Stewart, M., Vértessy, B. G., Forwood, J. K., & Kobe, B. (2016). Structural Biology and Regulation of Protein Import into the Nucleus. *Journal of Molecular Biology*, *428*(10), 2060–2090. doi: 10.1016/j.jmb.2015.10.023

Cope, G. A., Suh, G. S. B., Aravind, L., Schwarz, S. E., Zipursky, S. L., Koonin, E. V., & Deshaies, R. J. (2002). Role of predicted metalloprotease motif of Jab1/Csn5 in cleavage of Nedd8 from Cul1. *Science*, *298*(5593), 608–611. doi: 10.1126/science.1075901

Dirk, G., & Kutay, U. (1999). Transport between the cell nucleus and the cytoplasm. *Annual Reviews Cellular Development Biology*, *15*, 607–660.

Durrant, W. E., & Dong, X. (2004). Systemic acquired resistance. *Annual Review of Phytopathology*, *42*, 185–209. doi: 10.1146/annurev.phyto.42.040803.140421

Florentino, L. H., Santos, A. A., Fontenelle, M. R., Pinheiro, G. L., Zerbini, F. M., Baracat-Pereira, M. C., & Fontes, E. P. B. (2006). A PERK-Like Receptor Kinase Interacts with the Geminivirus Nuclear Shuttle Protein and Potentiates Viral Infection. *Journal of Virology*, *80*(13), 6648–6656. doi: 10.1128/jvi.00173-06

Fontes, E. P. B., Santos, A. A., Luz, D. F., Waclawovsky, A. J., & Chory, J. (2004). The geminivirus nuclear shuttle protein is a virulence factor that suppresses

transmembrane receptor kinase activity. *Genes and Development*, *18*(20), 2545–2556. doi: 10.1101/gad.1245904

Gaffney, T., Friedrich, L., Vernooij, B., Negrotto, D., Nye, G., Uknes, S., Ward, E., Kessmann, H., & Ryals, J. (1993). Requirement of salicylic acid for the induction of systemic acquired resistance. *Science*, *261*(5122), 754–756. doi: 10.1126/science.261.5122.754

Gafni, Y., & Epel, B. L. (2002). The role of host and viral proteins in intra- and inter-cellular trafficking of geminiviruses. *Physiological and Molecular Plant Pathology*, *60*(5), 231–241. doi: 10.1006/pmpp.2002.0402

Gilbertson, R. L., Batuman, O., Webster, C. G., & Adkins, S. (2015). Role of the Insect Supervectors Bemisia tabaci and Frankliniella occidentalis in the Emergence and Global Spread of Plant Viruses. *Annual Review of Virology*, *2*, 67–93. doi: 10.1146/annurev-virology-031413-085410

Gouveia-Mageste, B. C., Martins, L. G. C., Dal-Bianco, M., Machado, J. P. B., Da Silva, J. C. F., Kim, A. Y., Yazaki, J., Dos Santos, A. A., Ecker, J. R., & Fontes, E. P. B. (2021). A plant-specific syntaxin-6 protein contributes to the intracytoplasmic route for the begomovirus CabLCV. *Plant Physiology*, *187*(1), 158–173. doi: 10.1093/plphys/kiab252

Hanley-Bowdoin, L., Bejarano, E. R., Robertson, D., & Mansoor, S. (2013). Geminiviruses: Masters at redirecting and reprogramming plant processes. *Nature Reviews Microbiology*, *11*(11), 777–788. doi: 10.1038/nrmicro3117

Jin, D., Li, B., Deng, X. W., & Wei, N. (2014). Plant COP9 Signalosome subunit 5, CSN5. *Plant Science*, *224*, 54–61. doi: 10.1016/j.plantsci.2014.04.001

Kim, S. J., Fernandez-Martinez, J., Nudelman, I., Shi, Y., Zhang, W., Raveh, B., Herricks, T., Slaughter, B. D., Hogan, J. A., Upla, P., Chemmama, I. E., Pellarin, R., Echeverria, I., Shivaraju, M., Chaudhury, A. S., Wang, J., Williams, R., Unruh, J. R., Greenberg, C. H., … Rout, M. P. (2018). Integrative structure and functional anatomy of a nuclear pore complex. *Nature*, *555*(7697), 475–482. doi: 10.1038/nature26003

Kong, Q., Sun, T., Qu, N., Ma, J., Li, M., Cheng, Y. T., Zhang, Q., Wu, D., Zhang, Z., & Zhang, Y. (2016). Two redundant receptor-like cytoplasmic kinases function downstream of pattern recognition receptors to regulate activation of SA biosynthesis. *Plant Physiology*, *171*(2), 1344–1354. doi: 10.1104/pp.15.01954

Krapp, S., Greiner, E., Amin, B., Sonnewald, U., & Krenz, B. (2017). The stress granule

component G3BP is a novel interaction partner for the nuclear shuttle proteins of the nanovirus pea necrotic yellow dwarf virus and geminivirus abutilon mosaic virus. *Virus Research*, *227*, 6–14. doi: 10.1016/j.virusres.2016.09.021

Kwok, S. F., Solano, R., Tsuge, T., Chamovitz, D. A., Ecker, J. R., Matsui, M., & Deng, X. W. (1998). Arabidopsis homologs of a c-Jun coactivator are present both in monomeric form and in the COP9 complex, and their abundance is differentially affected by the pleiotropic cop/det/fus mutations. *Plant Cell*, *10*(11), 1779–1790. doi: 10.1105/tpc.10.11.1779

Lai, Y. S., Renna, L., Yarema, J., Ruberti, C., He, S. Y., & Brandizzi, F. (2018). Salicylic acid-independent role of NPR1 is required for protection from proteotoxic stress in the plant endoplasmic reticulum. *Proceedings of the National Academy of Sciences of the United States of America*, *115*(22), E5203–E5212. doi: 10.1073/pnas.1802254115

Lazarowitz, S. G., & Beachy, R. N. (1999). Viral movement proteins as probes for intracellular and intercellular trafficking in plants. *Plant Cell*, *11*(4), 535–548. doi: 10.1105/tpc.11.4.535

Lee, H. J., Park, Y. J., Seo, P. J., Kim, J. H., Sim, H. J., Kim, S. G., & Park, C. M. (2015). Systemic immunity requires SnRK2.8-mediated nuclear import of NPR1 in arabidopsis. *Plant Cell*, *27*(12), 3425–3438. doi: 10.1105/tpc.15.00371

Lewis, J. D., & Lazarowitz, S. G. (2010). Arabidopsis synaptotagmin SYTA regulates endocytosis and virus movement protein cell-to-cell transport. *Proceedings of the National Academy of Sciences of the United States of America*, *107*(6), 2491–2496. doi: 10.1073/pnas.0909080107

Li, B., Ferreira, M. A., Huang, M., Camargos, L. F., Yu, X., Teixeira, R. M., Carpinetti, P. A., Mendes, G. C., Gouveia-Mageste, B. C., Liu, C., Pontes, C. S. L., Brustolini, O. J. B., Martins, L. G. C., Melo, B. P., Duarte, C. E. M., Shan, L., He, P., & Fontes, E. P. B. (2019). The receptor-like kinase NIK1 targets FLS2/BAK1 immune complex and inversely modulates antiviral and antibacterial immunity. *Nature Communications*, *10*(1), 1–14. doi: 10.1038/s41467-019-12847-6

Li, R., Weldegergis, B. T., Li, J., Jung, C., Qu, J., Sun, Y., Qian, H., Tee, C., Van Loon, J. J. A., Dicke, M., Chua, N. H., Liu, S. S., & Ye, J. (2014). Virulence factors of geminivirus interact with MYC2 to subvert plant resistance and promote vector performance. *Plant Cell*, *26*(12), 4991–5008. doi: 10.1105/tpc.114.133181

Li, X., & Gu, Y. (2020). Structural and functional insight into the nuclear pore complex

and nuclear transport receptors in plant stress signaling. *Current Opinion in Plant Biology*, *58*, 60–68. doi: 10.1016/j.pbi.2020.10.006

Lozano-Durán, R., & Rodríguez-Bejarano, E. (2011). Mutation in Arabidopsis CSN5A partially complements the lack of Beet curly top virus pathogenicity factor L2. *Journal of Plant Pathology & Microbiology*, *02*(03), 3–5. doi: 10.4172/2157-7471.1000108

Lozano-Durán, R., Rosas-Díaz, T., Gusmaroli, G., Luna, A. P., Taconnat, L., Deng, X. W., & Bejarano, E. R. (2011). Geminiviruses subvert ubiquitination by altering CSN-mediated derubylation of SCF E3 ligase complexes and inhibit jasmonate signaling in Arabidopsis thaliana. *Plant Cell*, *23*(3), 1014–1032. doi: 10.1105/tpc.110.080267

Lu, D., Wu, S., Gao, X., Zhang, Y., Shan, L., & He, P. (2010). A receptor-like cytoplasmic kinase, BIK1, associates with a flagellin receptor complex to initiate plant innate immunity. *Proceedings of the National Academy of Sciences*, *107*(1), 496–501. doi: 10.1073/PNAS.0909705107

Luan, J. B., Yao, D. M., Zhang, T., Walling, L. L., Yang, M., Wang, Y. J., & Liu, S. S. (2013). Suppression of terpenoid synthesis in plants by a virus promotes its mutualism with vectors. *Ecology Letters*, *16*(3), 390–398. doi: 10.1111/ele.12055

Machado, J. P. B. (2011). Identificação e caracterização de alvos celulares da proteína NIG(NSP- Interacting GTPase). 85 f. Dissertação (Mestrado em Bioquímica e Biologia molecular de plantas; Bioquímica e Biologia molecular animal) - Universidade Federal de Viçosa

Ma, X., Claus, L. A. N., Leslie, M. E., Tao, K., Wu, Z., Liu, J., Yu, X., Li, B., Zhou, J., Savatin, D. V., Peng, J., Tyler, B. M., Heese, A., Russinova, E., He, P., & Shan, L. (2020). Ligand-induced monoubiquitination of BIK1 regulates plant immunity. *Nature*, *581*(7807), 199–203. doi: 10.1038/s41586-020-2210-3

Mariano, A. C., Andrade, M. O., Santos, A. A., Carolino, S. M. B., Oliveira, M. L., Baracat-Pereira, M. C., Brommonshenkel, S. H., & Fontes, E. P. B. (2004). Identification of a novel receptor-like protein kinase that interacts with a geminivirus nuclear shuttle protein. *Virology*, *318*(1), 24–31. doi: 10.1016/j.virol.2003.09.038

Martins, L. G. C., Raimundo, G. A. S., Ribeiro, N. G. A., Silva, J. C. F., Euclydes, N. C., Loriato, V. A. P., Duarte, C. E. M., & Fontes, E. P. B. (2020). A Begomovirus Nuclear Shuttle Protein-Interacting Immune Hub: Hijacking Host Transport

Activities and Suppressing Incompatible Functions. *Frontiers in Plant Science*, *11*(April), 1–8. doi: 10.3389/fpls.2020.00398

Maytal-Kivity, V., Reis, N., Hofmann, K., & Glickman, M. H. (2002). MPN+, a putative catalytic motif found in a subset of MPN domain proteinsfrom eukaryotes and prokaryotes, is critical for Rpn11 function. *BMC Biochemistry*, *3*, 1–12. doi: 10.1186/1471-2091-3-28

McGarry, R. C., Barron, Y. D., Carvalho, M. F., Hill, J. E., Gold, D., Cheung, E., Kraus, W. L., & Lazarowitz, S. G. (2003). A novel Arabidopsis acetyltransferase interacts with the geminivirus movement protein NSP. *Plant Cell*, *15*(7), 1605–1618. doi: 10.1105/tpc.012120

McInerney, G. M. (2015). FGDF Motif Regulation of Stress Granule Formation. *DNA and Cell Biology*, *34*(9), 557–560. doi: 10.1089/dna.2015.2957

Merlet, J., Burger, J., Gomes, J. E., & Pintard, L. (2009). Regulation of cullin-RING E3 ubiquitin-ligases by neddylation and dimerization. *Cellular and Molecular Life Sciences*, *66*(11–12), 1924–1938. doi: 10.1007/s00018-009-8712-7

Mir, R., & León, J. (2014). Pathogen and Circadian Controlled 1 (PCC1) protein is anchored to the plasma membrane and interacts with subunit 5 of COP9 signalosome in Arabidopsis. *PLoS ONE*, *9*(1). doi: 10.1371/journal.pone.0087216

Mukhtar, M. S., Carvunis, A., Dreze, M., Epple, P., Steinbrenner, J., Moore, J., Tasan, M., Galli, M., Hao, T., Nishimura, M. T., Pevzner, S. J., Donovan, S. E., Ghamsari, L., Santhanam, B., Romero, V., Poulin, M. M., Gebreab, F., Gutierrez, B. J., Tam, S., … Beynon, J. (2011). Plant Immune System Network. *Science*, *333*(July), 596–601. doi: 10.1126/science.1203659.Independently

Noueiry, A. O., Lucas, W. J., & Gilbertson, R. L. (1994). Two proteins of a plant DNA virus coordinate nuclear and plasmodesmal transport. *Cell*, *76*(5), 925–932. doi: 10.1016/0092-8674(94)90366-2

Panas, M. D., Schulte, T., Thaa, B., Sandalova, T., Kedersha, N., Achour, A., & McInerney, G. M. (2015). Viral and Cellular Proteins Containing FGDF Motifs Bind G3BP to Block Stress Granule Formation. *PLoS Pathogens*, *11*(2), 1–22. doi: 10.1371/journal.ppat.1004659

Panas, M. D., Varjak, M., Lulla, A., Eng, K. E., Merits, A., Hedestam, G. B. K., & McInerney, G. M. (2012). Sequestration of G3BP coupled with efficient translation inhibits stress granules in Semliki Forest virus infection. *Molecular Biology of the Cell*, *23*(24), 4701–4712. doi: 10.1091/mbc.E12-08-0619

Park, S. W., Kaimoyo, E., Kumar, D., Mosher, S., & Klessig, D. F. (2007). Methyl salicylate is a critical mobile signal for plant systemic acquired resistance. *Science*, *318*(5847), 113–116. doi: 10.1126/science.1147113

Pilartz, M., & Jeske, H. (1992). Abutilon mosaic geminivirus double-stranded DNA is packed into minichromosomes. *Virology*, *189*(2), 800–802. doi: 10.1016/0042-6822(92)90610-2

Pilartz, M., & Jeske, H. (2003). Mapping of Abutilon Mosaic Geminivirus Minichromosomes. *Journal of Virology*, *77*(20), 10808–10818. doi: 10.1128/jvi.77.20.10808-10818.2003

Qi, G., Chen, J., Chang, M., Chen, H., Hall, K., Korin, J., Liu, F., Wang, D., & Fu, Z. Q. (2018). Pandemonium Breaks Out: Disruption of Salicylic Acid-Mediated Defense by Plant Pathogens. *Molecular Plant*, *11*(12), 1427–1439. doi: 10.1016/j.molp.2018.10.002

Rabut, G., & Peter, M. (2008). Function and regulation of protein neddylation. "Protein modifications: beyond the usual suspects" review series. *EMBO Reports*, *9*(10), 969–976. doi: 10.1038/embor.2008.183

Ribbeck, K., Lipowsky, G., Kent, H. M., Stewart, M., & Görlich, D. (1998). NTF2 mediates nuclear import of Ran. *EMBO Journal*, *17*(22), 6587–6598. doi: 10.1093/emboj/17.22.6587

Rocha, C. S., Santos, A. A., Machado, J. P. B., & Fontes, E. P. B. (2008). The ribosomal protein L10/QM-like protein is a component of the NIK-mediated antiviral signaling. *Virology*, *380*(2), 165–169. doi: 10.1016/j.virol.2008.08.005

Rojas, M. R. (1993). Use of Degenerate Primers in the Polymerase Chain Reaction to Detect Whitefly-Transmitted Geminiviruses. *Plant Disease*, *77*(4), 340. doi: 10.1094/pd-77-0340

Rojas, M. R., Hagen, C., Lucas, W. J., & Gilbertson, R. L. (2005). Exploiting chinks in the plant's armor: Evolution and emergence of geminiviruses. *Annual Review of Phytopathology*, *43*, 361–394. doi: 10.1146/annurev.phyto.43.040204.135939

Rojas, M. R., Macedo, M. A., Maliano, M. R., Soto-Aguilar, M., Souza, J. O., Briddon, R. W., Kenyon, L., Rivera Bustamante, R. F., Zerbini, F. M., Adkins, S., Legg, J. P., Kvarnheden, A., Wintermantel, W. M., Sudarshana, M. R., Peterschmitt, M., Lapidot, M., Martin, D. P., Moriones, E., Inoue-Nagata, A. K., & Gilbertson, R. L. (2018). World Management of Geminiviruses. *Annual Review of Phytopathology*, *56*, 637–677. doi: 10.1146/annurev-phyto-080615-100327

Sánchez-Velar, N., Udofia, E. B., Yu, Z., & Zapp, M. L. (2004). hRIP, a cellular cofactor for Rev function, promotes release of HIV RNAs from the perinuclear region. *Genes and Development*, *18*(1), 23–34. doi: 10.1101/gad.1149704

Sakamoto, T., Deguchi, M., Brustolini, O. J. B., Santos, A. A., Silva, F. F., & Fontes, E. P. B. (2012). The tomato RLK superfamily: Phylogeny and functional predictions about the role of the LRRII-RLK subfamily in antiviral defense. *BMC Plant Biology*, *12*. doi: 10.1186/1471-2229-12-229

Sanderfoot, A. A., & Lazarowitz, S. G. (1995). Cooperation in viral movement: The geminivirus BL1 movement protein interacts with BR1 and redirects it from the nucleus to the cell periphery. *Plant Cell*, *7*(8), 1185–1194. doi: 10.1105/tpc.7.8.1185

Santos, A. A., Carvalho, C. M., Florentino, L. H., Ramos, H. J. O., & Fontes, E. P. B. (2009). Conserved threonine residues within the A-loop of the receptor NIK differentially regulate the kinase function required for antiviral signaling. *PLoS ONE*, *4*(6). doi: 10.1371/journal.pone.0005781

Schwechheimer, C., & Isono, E. (2010). The COP9 signalosome and its role in plant development. *European Journal of Cell Biology*, *89*(2–3), 157–162. doi: 10.1016/j.ejcb.2009.11.021

Smith, A., Brownawell, A., & Macara, I. G. (1998). Nuclear import of Ran is mediated by the transport factor NTF2. *Current Biology*, *8*(25), 1403–1406. doi: 10.1016/s0960-9822(98)00023-2

Spoel, S. H., Koornneef, A., Claessens, S. M. C., Korzelius, J. P., Van Pelt, J. A., Mueller, M. J., Buchala, A. J., Métraux, J. P., Brown, R., Kazan, K., Van Loon, L. C., Dong, X., & Pieterse, C. M. J. (2003). NPR1 modulates cross-talk between salicylate- and jasmonate-dependent defense pathways through a novel function in the cytosol. Plant Cell, 15(3), 760–770. doi: 10.1105/tpc.009159

Spoel, S. H., Mou, Z., Tada, Y., Spivey, N. W., Genschik, P., & Dong, X. (2009). Proteasome-Mediated Turnover of the Transcription Coactivator NPR1 Plays Dual Roles in Regulating Plant Immunity. *Cell*, *137*(5), 860–872. doi: 10.1016/j.cell.2009.03.038

Tamura, K., & Hara-Nishimura, I. (2014). Functional insights of nucleocytoplasmic transport in plants. *Frontiers in Plant Science*, *5*(APR), 1–10. doi: 10.3389/fpls.2014.00118

Tan, S., Abas, M., Verstraeten, I., Glanc, M., Molnár, G., Hajný, J., Lasák, P., Petřík,

I., Russinova, E., Petrášek, J., Novák, O., Pospíšil, J., & Friml, J. (2020). Salicylic Acid Targets Protein Phosphatase 2A to Attenuate Growth in Plants. *Current Biology*, *30*(3), 381-395.e8. doi: 10.1016/j.cub.2019.11.058

Teixeira, R. M., Ferreira, M. A., Raimundo, G. A. S., Loriato, V. A. P., Reis, P. A. B., & Fontes, E. P. B. (2019). Virus perception at the cell surface: revisiting the roles of receptor-like kinases as viral pattern recognition receptors. *Molecular Plant Pathology*, *20*(9), 1196–1202. doi: 10.1111/mpp.12816

Terrence P. Delaney, Scott Uknes, Bernard Vernooij, Leslie Friedrich, Kris Weymann, D. N., & Thomas Gaffney, Manuela Gut-Rella, Helmut Kessmann, Eric Ward, J. R. (1994). *A Central Role of Salicylic Acid in Plant Disease Resistanc*. *266*(November), 1247–1250.

Thran, M., Link, K., & Sonnewald, U. (2012). The Arabidopsis DCP2 gene is required for proper mRNA turnover and prevents transgene silencing in Arabidopsis. *Plant Journal*, *72*(3), 368–377. doi: 10.1111/j.1365-313X.2012.05066.x

Tourrière, H., Chebli, K., Zekri, L., Courselaud, B., Blanchard, J. M., Bertrand, E., & Tazi, J. (2003). The RasGAP-associated endoribonuclease G3BP assembles stress granules. *Journal of Cell Biology*, *160*(6), 823–831. doi: 10.1083/jcb.200212128

Verma, R., Aravind, L., Oania, R., McDonald, W. H., Yates, J. R., Koonin, E. V., & Deshaies, R. J. (2002). Role of Rpn11 metalloprotease in deubiquitination and degradation by the 26S proteasome. *Science*, *298*(5593), 611–615. doi: 10.1126/science.1075898

Wei, N., & Deng, X. W. (2003). The COP9 Signalosome. *Annual Review of Cell and Developmental Biology*, *19*, 261–286. doi: 10.1146/annurev.cellbio.19.111301.112449

Wei, N., Serino, G., & Deng, X. W. (2008). The COP9 signalosome: more than a protease. *Trends in Biochemical Sciences*, *33*(12), 592–600. doi: 10.1016/j.tibs.2008.09.004

White, J. P., Cardenas, A. M., Marissen, W. E., & Lloyd, R. E. (2007). Inhibition of Cytoplasmic mRNA Stress Granule Formation by a Viral Proteinase. *Cell Host and Microbe*, *2*(5), 295–305. doi: 10.1016/j.chom.2007.08.006

Wiermer, M., Feys, B. J., & Parker, J. E. (2005). Plant immunity: The EDS1 regulatory node. *Current Opinion in Plant Biology*, *8*(4), 383–389. doi: 10.1016/j.pbi.2005.05.010

Xiaoxia, L., Zhang, J., Jinkai, S., Ying, L., & Guodong, R. (2019). The Salix SmSPR1 Involved in Light-Regulated Cell Expansion by Modulating Microtubule Arrangement. *Frontiers in Cell and Developmental Biology*, *7*(November), 1–14. doi: 10.3389/fcell.2019.00309

Xu, J., Yang, J. Y., Niu, Q. W., & Chua, N. H. (2006). Arabidopsis DCP2, DCP1, and VARICOSE form a decapping complex required for postembryonic development. *Plant Cell*, *18*(12), 3386–3398. doi: 10.1105/tpc.106.047605

Yamaguchi, N., Winter, C. M., Wu, M.-F., Kwon, C. S., William, D. A., & Wagner, D. (2014). PROTOCOL: Chromatin Immunoprecipitation from Arabidopsis Tissues. *The Arabidopsis Book*, *12*, e0170. doi: 10.1199/tab.0170

Yazaki, J., Galli, M., Kim, A. Y., Nito, K., Aleman, F., Chang, K. N., Carvunis, A. R., Quan, R., Nguyen, H., Song, L., Alvarez, J. M., Huang, S. S. C., Chen, H., Ramachandran, N., Altmann, S., Gutiérrez, R. A., Hill, D. E., Schroeder, J. I., Chory, J., LaBaerl, J., Vidale, M., Braunj, P., Ecker, J. R. (2016). Mapping transcription factor interactome networks using HaloTag protein arrays. *Proceedings of the National Academy of Sciences of the United States of America*, *113*(29), E4238–E4247. doi: 10.1073/pnas.1603229113

Ye, J., Yang, J., Sun, Y., Zhao, P., Gao, S., Jung, C., Qu, J., Fang, R., & Chua, N. H. (2015). Geminivirus Activates ASYMMETRIC LEAVES 2 to Accelerate Cytoplasmic DCP2-Mediated mRNA Turnover and Weakens RNA Silencing in Arabidopsis. *PLoS Pathogens*, *11*(10), 1–21. doi: 10.1371/journal.ppat.1005196

Zavaliev, R., Mohan, R., Chen, T., & Dong, X. (2020). Formation of NPR1 Condensates Promotes Cell Survival during the Plant Immune Response. *Cell*, *182*(5), 1093-1108.e18. doi: 10.1016/j.cell.2020.07.016

Zerbini, F. M., Briddon, R. W., Idris, A., Martin, D. P., Moriones, E., Navas-Castillo, J., Rivera-Bustamante, R., Roumagnac, P., & Varsani, A. (2017). ICTV virus taxonomy profile: Geminiviridae. *Journal of General Virology*, *98*(2), 131–133. doi: 10.1099/jgv.0.000738

Zhang, J., Gao, J., Zhu, Z., Song, Y., Wang, X., Wang, X., & Zhou, X. (2020). MKK4/MKK5-MPK1/MPK2 cascade mediates SA-activated leaf senescence via phosphorylation of NPR1 in Arabidopsis. *Plant Molecular Biology*, *102*(4–5), 463–475. doi: 10.1007/s11103-019-00958-z

Zhang, Y., & Li, X. (2019). Salicylic acid: biosynthesis, perception, and contributions to plant immunity. *Current Opinion in Plant Biology*, *50*, 29–36. doi:

10.1016/j.pbi.2019.02.004

Zhang, X., Henriques, R., Lin, S. S., Niu, Q. W., & Chua, N. H. (2006). Agrobacterium-mediated transformation of Arabidopsis thaliana using the floral dip method. Nature Protocols, 1(2), 641–646. doi: 10.1038/nprot.2006.97

Zhou, X., Boruc, J., & Meier, I. (2013). The Plant Nuclear Pore Complex - The Nucleocytoplasmic Barrier and Beyond. In Annual Plant Reviews online (Vol. 46). doi: 10.1002/9781119312994.apr0499

Zhou, Y., Rojas, M. R., Park, M.-R., Seo, Y.-S., Lucas, W. J., & Gilbertson, R. L. (2011). Histone H3 Interacts and Colocalizes with the Nuclear Shuttle Protein and the Movement Protein of a Geminivirus. *Journal of Virology*, *85*(22), 11821–11832. doi: 10.1128/jvi.00082-11

Zorzatto, C., Machado, J. P. B., Lopes, K. V. G., Nascimento, K. J. T., Pereira, W. A., Brustolini, O. J. B., Reis, P. A. B., Calil, I. P., Deguchi, M., Sachetto-Martins, G., Gouveia, B. C., Loriato, V. A. P., Silva, M. A. C., Silva, F. F., Santos, A. A., Chory, J., & Fontes, E. P. B. (2015). NIK1-mediated translation suppression functions as a plant antiviral immunity mechanism. *Nature*, *520*(7549), 679–682. doi: 10.1038/nature14171

SUPPLEMENTARY DATA

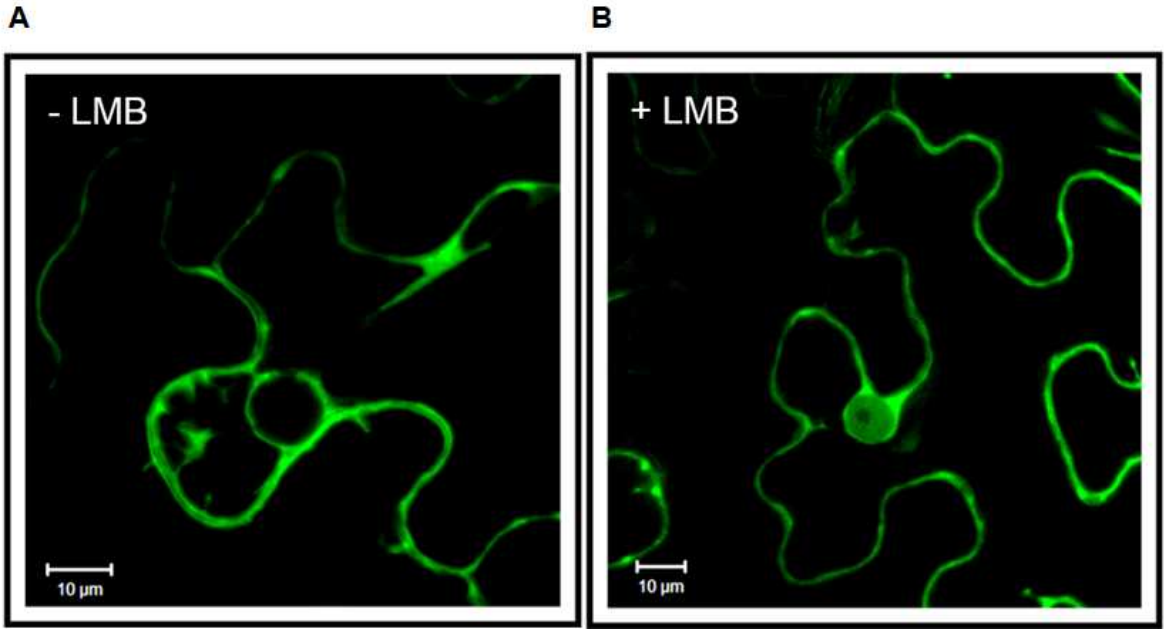

Supplementary Figure 1. NIG can be rellocated to the nucleus upon Leptomycin B treatment.

Nicotiana benthamiana leaves were agroinfiltrated with NIG-GFP and the 100nM Leptomycin B diluted in 100mM MES and 10mM $MgCl_2$ was applied 3 h before analysis. The epidermal cells of agroinfiltrated areas were analyzed after 72 hours with a Zeiss inverted LSM510 META laser scanning microscope equipped with argon and helium lasers as excitation sources. The NIG-GFP fusion protein was excited at 488 nm with the argon laser, and GFP emission was detected using a 500-530 nm filter. The images were captured and processed with the Zeiss LSM Image Browser 4 software.

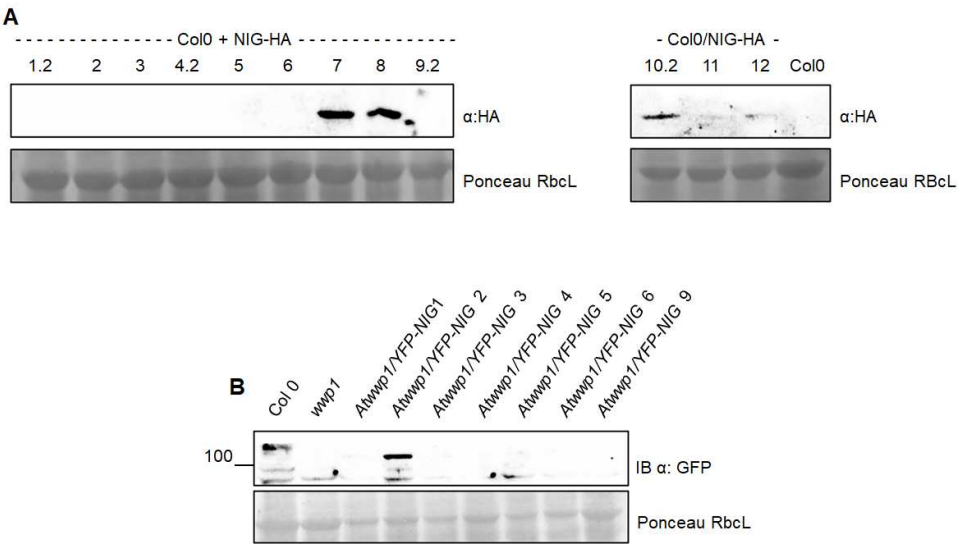

Supplementary Figure 2.Protein expression in Arabidopsis thaliana transgenic lines.

A. NIG-HA protein accumulation in Col0 plants stably transformed with 2x35S::NIG-HA. **B.** YFP-NIG protein accumulation in *atwwp1* plants stably transformed with 35S::YFP-NIG.

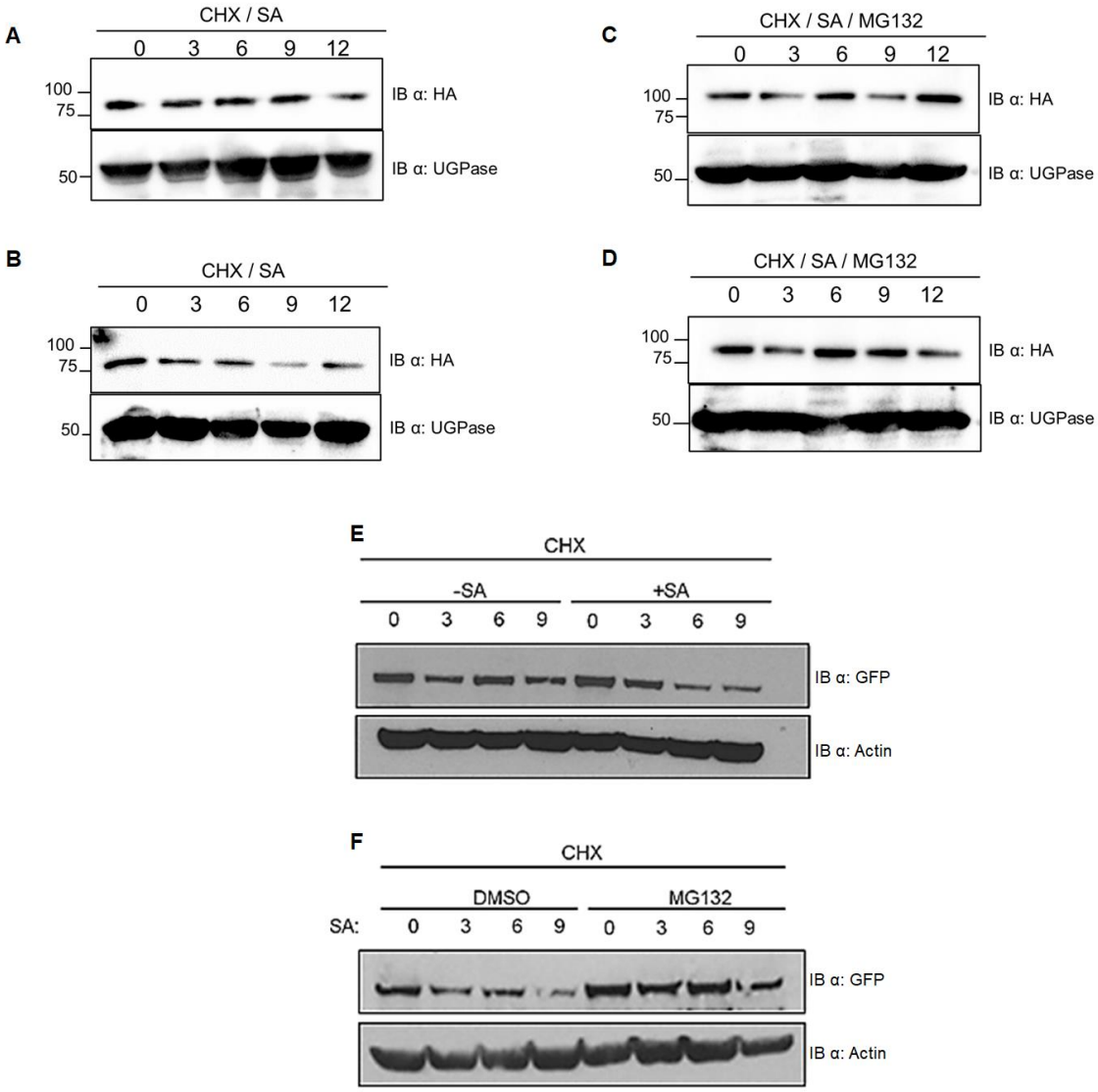

Supplementary Figure 3. Supplementary Figure 3. Salicylic acid induces NIG degradation.

A-B. NIG-HA is degraded at 9 h of SA 500 µM treatment. The blots show the results of independent assays. **C-D.** NIG-HA homeostasis is not affected by SA in samples supplemented with the proteasome inhibitor MG132 30 µM. UGPase was used as an endogenous loading control. Col0/2x35S::NIG-HA plants were utilized. **E.** NIG-GFP homeostasis is affected at 6 h of 500 µM SA treatment **F.** 30 µM MG132 inhibits the SA-mediated degradation of NIG-GFP. Actin was used as an endogenous loading control. Col0/35S::NIG-GFP plants were utilized. The protein synthesis inhibitor cycloheximide (CHX) 100 µM was used in all assays.

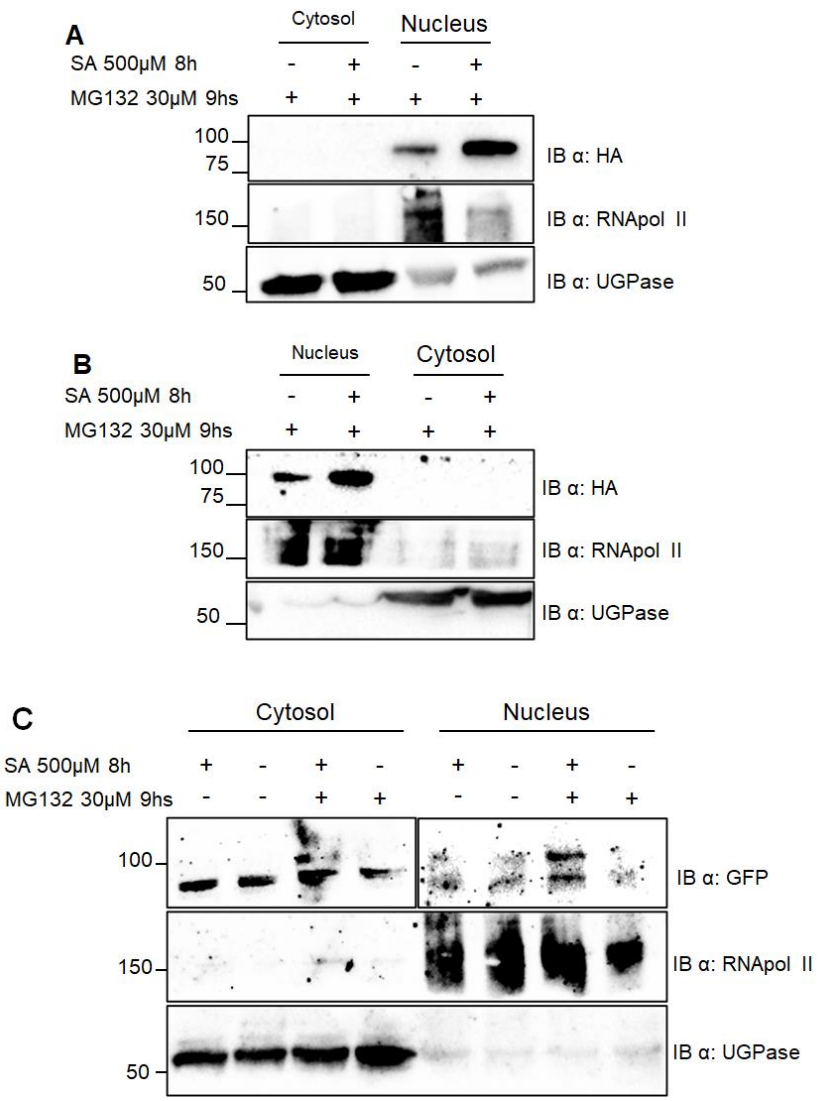

Supplementary Figure 4. NIG is redirected to the nucleus by SA.

A-B. NIG-HA is relocated to the nucleus upon SA treatment. Col0/2x35S::NIG-HA plants were utilized. **C.** NIG-GFP levels increase in the nuclear fraction upon SA treatment. Col0/35S::NIG-GFP plants were utilized. For all assays, the cytosolic protein UGPase and the nuclear protein RNApolII were utilized as endogenous controls for loading and contamination between fractions.

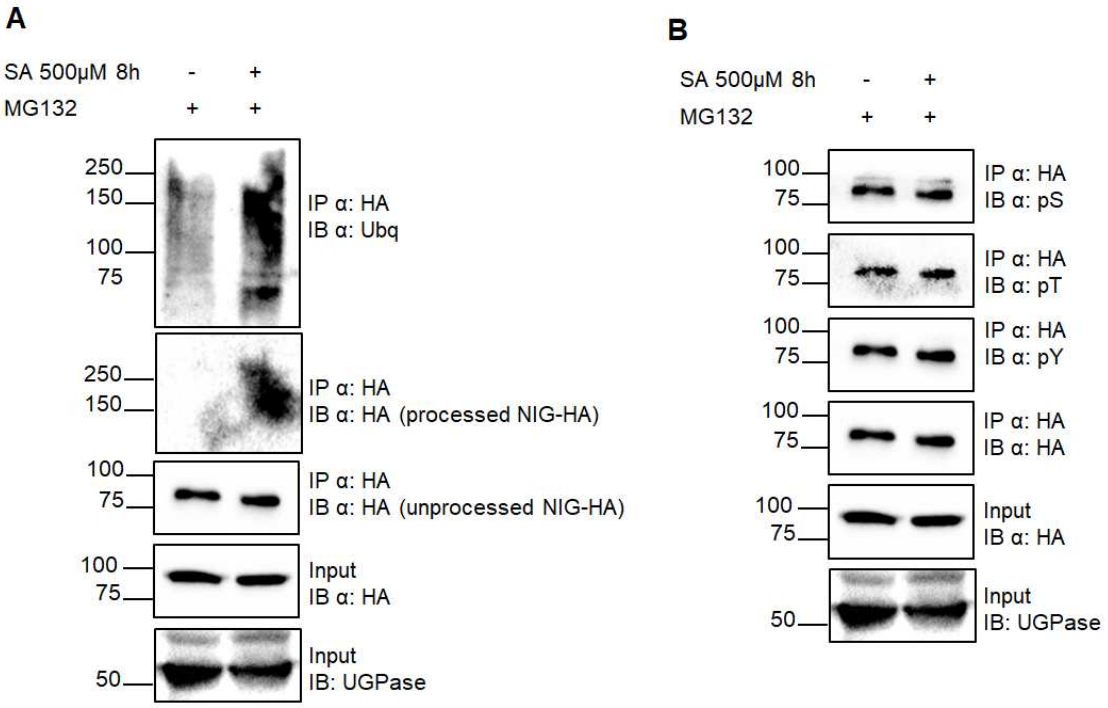

Supplementary Figure 5. NIG-HA post-translational modifications.

A. NIG-HA is polyubiquitinated upon SA treatment. **B.** NIG-HA is phosphorylated in serine, threonine and tyrosine residues with or without SA treatment. Col0/2x35S::NIG-HA plants were utilized. The protein UGPase was used as a loading control for the input.

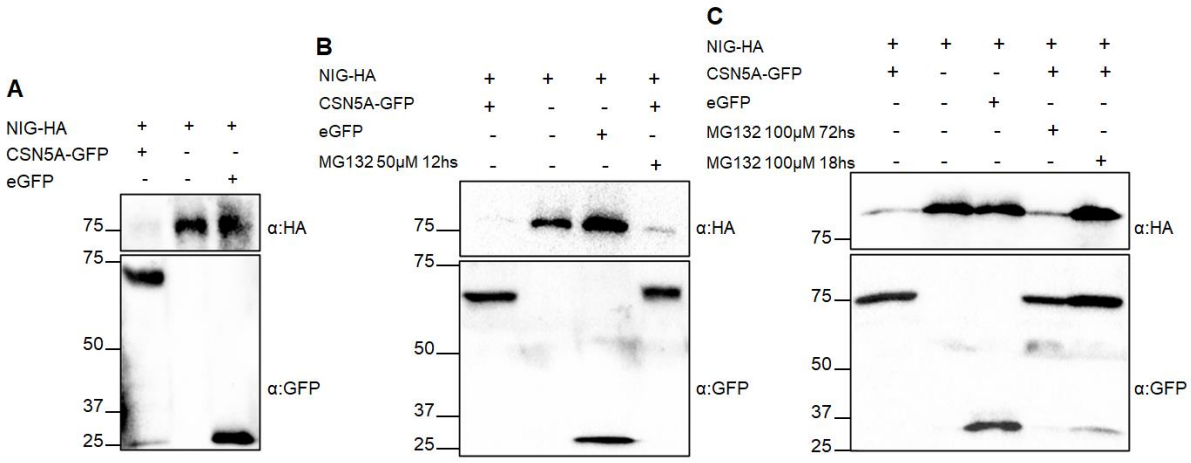

Supplementary Figure 6. CSN5A induces NIG degradation.

A-B. Attempts to sufficiently express NIG in the presence of CSN5A. **C.** The proteasome inhibitor MG132 is capable to inhibit the CSN5A-mediated turnover of NIG when plants are treated with MG132 100 μM for 18 h. The indicated constructs were transiently expressed in *N.benthamiana.*

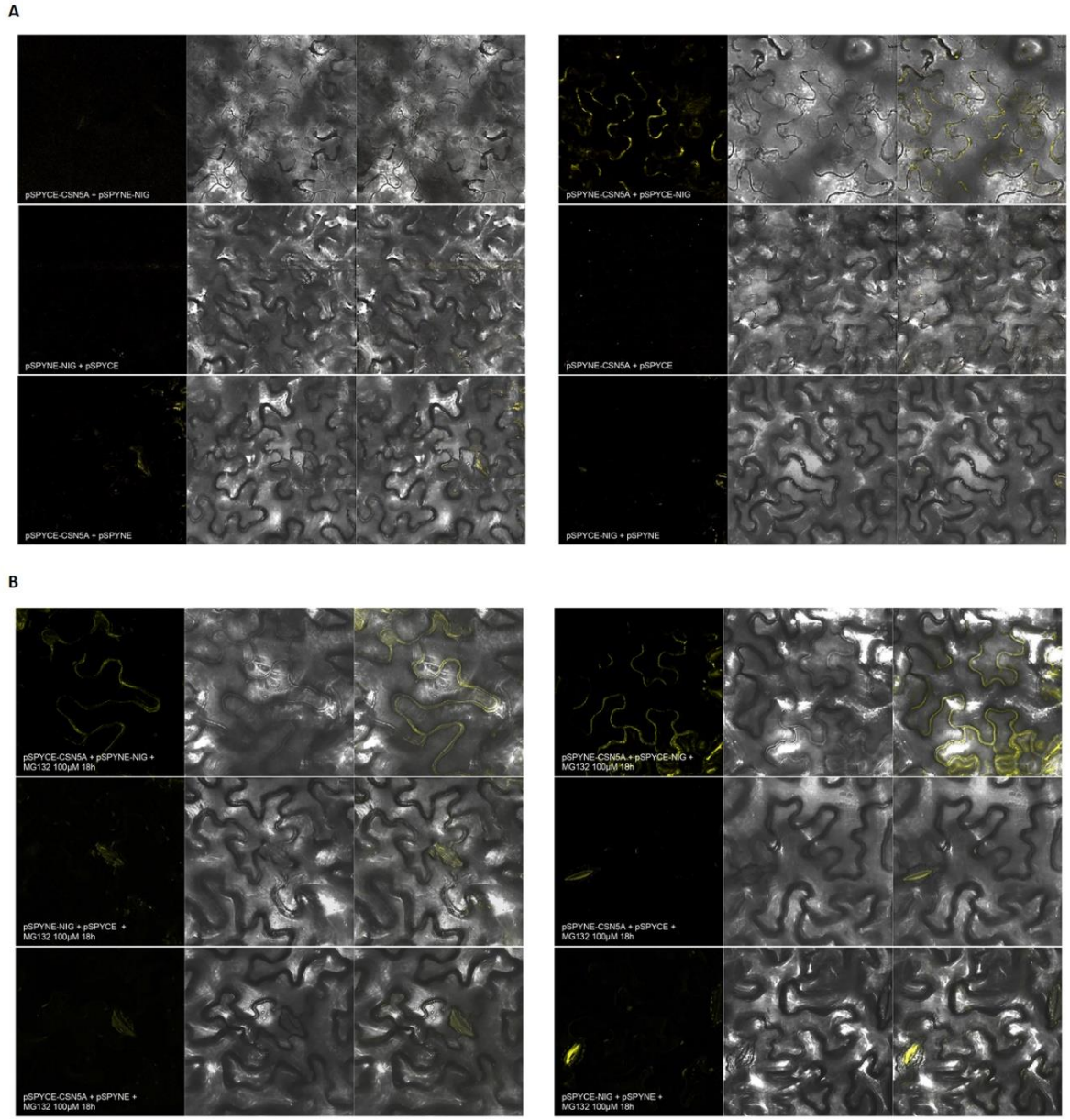

Supplementary Figure 7. Interactions and negative controls of NIG and CSN5A BiFC assay.

A-B. *In vivo* interaction between NIG and CSN5A by bimolecular fluorescence complementation (BiFC) analysis. The interaction of NIG-SPYCE and CSN5A-SPYNE combination was only observed in samples pre-treated with MG132 100 µM (**B**)**.** The YFP fluorescence was evaluated in *Nicotiana benthamiana* leaves co-infiltrated with 35S::NIG-SPYNE + 35S::CSN5A-SPYCE, 35S::NIG-SPYCE + 35S::CSN5A-SPYNE fusion proteins. The negative controls were pSPYNE + 35S::CSN5A-SPYCE, pSPYCE + 35S::CSN5A-SPYNE, 35S::NIG-SPYNE + pSPYCE and 35S::NIG-SPYCE + pSPYNE.

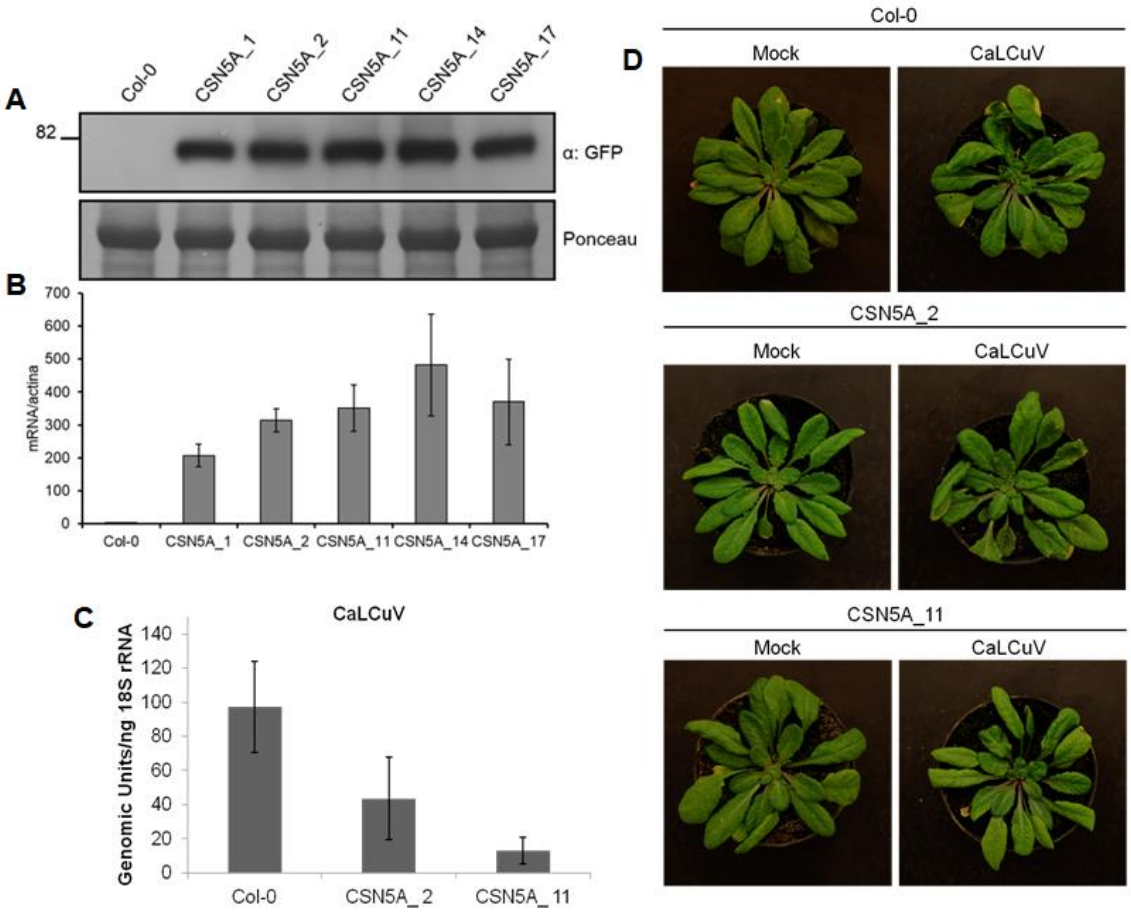

Supplementary Figure 8. CSN5A overexpression leads to enhanced resistance to CabCLV.

A. Accumulation of CSN5A-GFP protein in 5 transgenic complemented lines. Total protein was extracted from the indicated genotype and CSN5A was immunoblotted using anti-GFP. The Col-0 extract was used as negative control. **B.** Transcript accumulation of CSN5A-GFP transcripts in Col-0 and 5 transgenic overexpressing lines (Col0/35S::CSN5A-GFP). The levels of CSN5A transcript were determined by RT-qPCR using actin as an endogenous control. **C.** vDNA accumulation was determined by qPCR. The 18S ribosomal RNA was used as template for normalization. **D.** Phenotypes of CabCLV-infected plants. Col-0*, Col0/35S::CSN5A-GFP 2* and 11 lines are represented.

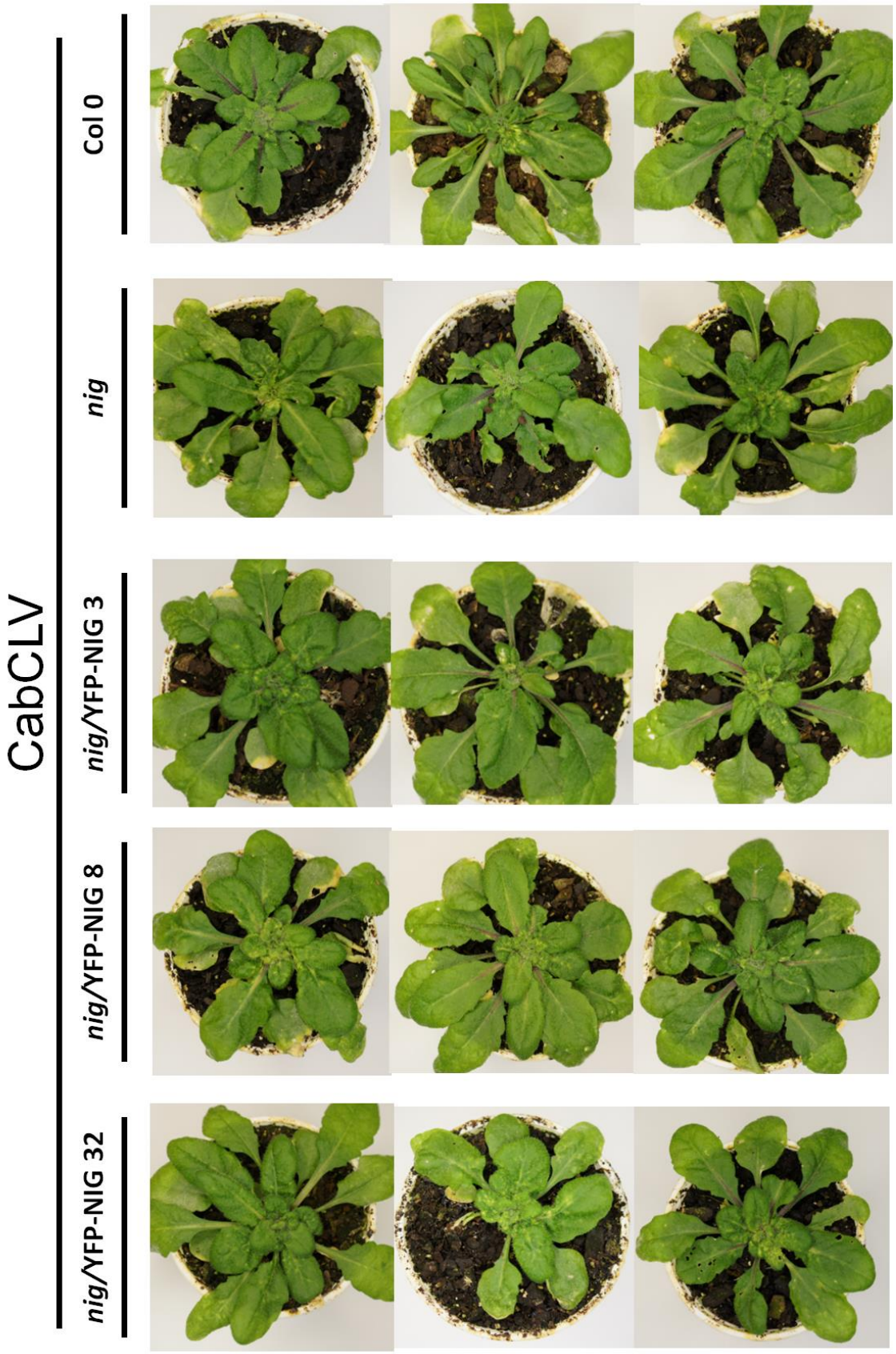

Supplementary Figure 9. Phenotypes of CabCLV-infected plants.

Col-0, nig and 3 *nig*/YFP-NIG independent lines are represented. Photography was taken 14 d.p.i (days post infection).

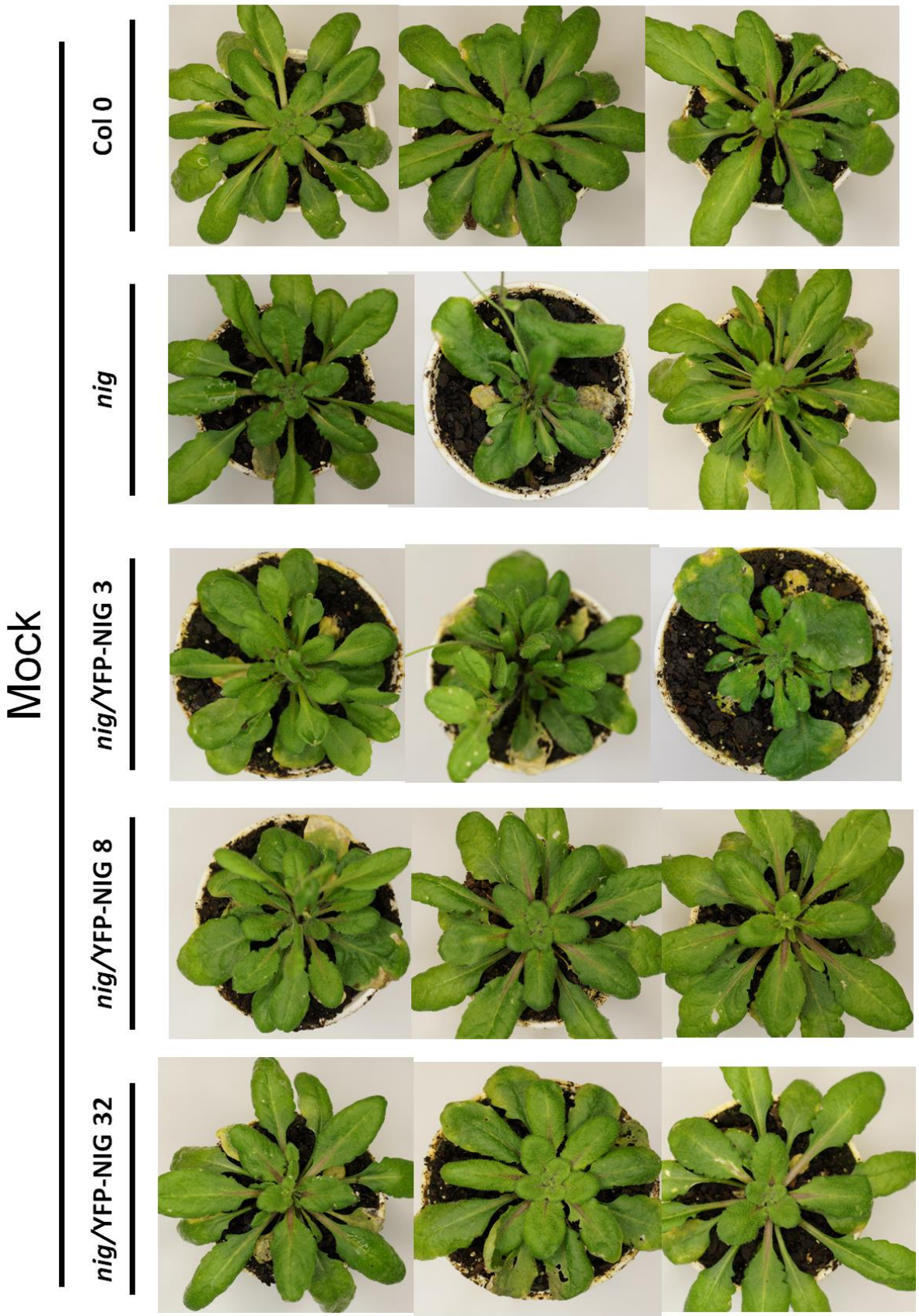

Supplementary Figure 10. Phenotypes of Mock-inoculated plants.

Col-0, nig and 3 *nig*/YFP-NIG independent lines are represented. Photography was taken 14 -days after mock inoculation.

Name	Gene/Flanking Sequence	Sequence (5' → 3')
35S_MC36-Fwd	CaMV 35S promoter (Fwd)	TCCTTCGCAAGACCCTTCCTC
ArfGAPNIG-ST-Rvs	ArfGAPNIG domain	AGAAAGCTGGGTCTTACTTATCATCATTCTTCTC
CSN5A-NS-Rvs	CSN5A	AGAAAGCTGGGTCCGATGTAATCATGGGCTC
qRT_CaLCuV-Fwd	CaLCuV DNA-B	GGGCCTGGGCCTGTTAGT
qRT_CaLCuV-Rvs	CaLCuV DNA-B	ACGGAAGATGGGAGAGGAAGA
qRT_18SRNA-Fwd	Arabidopsis thaliana 18SRNA	TTTGCGCGCCTGCTGCC
qRT_18SRNAVRvs	Arabidopsis thaliana 18SRNA	TGTGCTGGCGACGCATCATT
PBL1v2040	Begomovirus-specific primers (Rojas *et al.*, 1993)	GCCTCTGCAGCARTGRTCKATCTTCATA CA
PCRC1	Begomovirus-specific primers (Rojas *et al.*, 1993)	CTAGCTGCAGCATATTTACRARWATGC CA
qRTCSN5AFWD	CSN5A cDNA	TGTTCAATTCCGCTCGTCAG
qRTCSN5ARVS	CSN5A cDNA	TCACGATGTAATCATGGGCTC
qRTNIGFWD	NIG cDNA	TAAATGTATCGCAACCACCAC
qRTNIGRVS	NIG cDNA	AGAAGAAGTCACTGCCAACTG

Supplementary Table 1. Primer names and corresponding sequences.